MICROSTRUCTURE, *IN VITRO* DEGRADATION BEHAVIOUR AND ANTIMICROBIAL PROPERTIES OF COBALT DOPED DICALCIUM PHOSPHATE BONE CEMENTS

Betül SARSIK

2021
MASTER THESIS
BIOMEDICAL ENGINEERING

THESIS ADVISOR

Assist.Prof.Dr. Ammar Zeidan Ghailan ALSHEMARY

MICROSTRUCTURE, *IN VITRO* DEGRADATION BEHAVIOUR AND ANTIMICROBIAL PROPERTIES OF COBALT DOPED DICALCIUM PHOSPHATE BONE CEMENTS

Betül SARSIK

T.C.

Karabuk University

Institute of Graduate Programs

Department of Biomedical Engineering

Prepared as

Master Thesis

Thesis Advisor

Assist.Prof.Dr. Ammar Zeidan Ghailan ALSHEMARY

KARABUK

July 2021

I certify that in my opinion the thesis submitted by Betül SARSIK titled "MICROSTRUCTURE, *IN VITRO* DEGRADATION BEHAVIOUR AND ANTIMICROBIAL PROPERTIES OF COBALT DOPED DICALCIUM PHOSPHATE BONE CEMENTS" is fully adequate in scope and in quality as a thesis for the degree of Master of Science.

Assist.Prof.Dr. Ammar Zeidan Ghailan ALSHEMARY .....
Thesis Advisor, Department of Biomedical Engineering

This thesis is accepted by the examining committee with a unanimous vote in the Department of Biomedical Engineering as a Master of Science thesis. July 1, 2021

Examining Committee Members (Institutions)	Signature
Chairman : Assist. Prof. Dr. Ali Deniz DALGIÇ (BİLGİ U.)	.....
Member : Assist. Prof. Dr. Daver Ali (KBU)	.....
Member : Assist. Prof. Dr. Ammar Zeidan Ghailan ALSHEMARY (KBU)	

The degree of Master of Science by the thesis submitted is approved by the Administrative Board of the Institute of Graduate Programs, Karabuk University.

Prof. Dr. Hasan SOLMAZ .....
Director of the Institute of Graduate Programs

"I declare that all the information within this thesis has been gathered and presented in accordance with academic regulations and ethical principles and I have according to the requirements of these regulations and principles cited all those which do not originate in this work as well."

Betül SARSIK

ABSTRACT

M. Sc. Thesis

MICROSTRUCTURE, *IN VITRO* DEGRADATION BEHAVIOUR AND ANTIMICROBIAL PROPERTIES OF COBALT DOPED DICALCIUM PHOSPHATE BONE CEMENTS

Betül SARSIK

Karabük University
Institute of Graduate Programs
The Department of Biomedical Engineering

Thesis Advisor:
Assist. Prof. Dr. Ammar Zeidan Ghailan ALSHEMARY
July, 48 pages

Repair of bone defects is a problem in orthopedics and traumatology operations. In bone treatments, biomaterials need to prevent bacterial infections and make bone treatment more accessible. In the first part of this study, pure phase of β-tricalcium phosphate (βTCP) and cobalt substituted βTCP (Co-βTCP) materials were synthesized using microwave-assisted wet precipitation method. The prepared powders were characterized using X-ray powder diffraction (XRD), Fourier-transform infrared spectroscopy (FTIR), and Scanning electron microscope (SEM) techniques to verify both Co^{2+} doping and to explore the alterations in the structural and molecular properties upon doping. With the incorporation of Co^{2+} ions, the lattice parameters, degree of crystallinity, and particle size of βTCP were significantly decreased. The functional groups of βTCP (or Co-βTCP) were detected via the FTIR technique. The optical properties of βTCP (or Co-βTCP) were

evaluated using Ultraviolet-visible spectrophotometry (UV–Vis). Two bands located at 530 and 678 nm were observed for Co-βTCP materials. In the second part of this study, dicalcium phosphate (DCP) and Co modified DCP (La-DCP) bone cements were made based on acid/base reaction between βTCP (or Co-βTCP) and monocalcium phosphate monohydrate (MCPM) in the presence of water. The obtained bone cements were characterized using XRD, FTIR, and SEM techniques. The DCP cements existed as a monetite phase. The a and b axis of monetite crystals increased with the addition of Co^{2+} ions, while the degree of crystallinity and crystallite size significantly decreased with an increasing amount of Co^{2+} ions in the DCP structure. In vitro degradation of DCP and Co-DCP bone cements was examined using Phosphate buffered saline (PBS) over 14 days at 37 ºC. The degradation of DCP bone cements was controlled with the incorporation of Co^{2+} ions. Antibacterial properties of pure and Co doped DCP bone cements were evaluated qualitatively against Escherichia coli (E. Coli), Methicillin-sensitive Staphylococcus aureus (MSSA). Methicillin-resistant Staphylococcus aureus (MRSA), Methicillin-resistant coagulase negative staphylococci (MR-CoNS), and Pseudomonas aeruginosa (P. aeruginosa) bacteria for 24 h at 37 ºC. The results showed that the addition of Co^{2+} ions inhibited the growth of E.coli and MSSA bacteria. The prepared bone cements with antibacterial properties would be a promising material for inhibiting any infection-causing failure in bone repair.

Key Words : Bone cements, Dicalcium phosphate, Cobalt, Characterizations, Antibacterial properties.

Science Code : 92503

ÖZET

Yüksek Lisans Tezi

KOBALT KATKILI DİKALSİYUM FOSFAT KEMİK ÇİMENTOLARININ MİKRO YAPISI, *İN VİTRO* BOZUNMA DAVRANIŞI VE ANTİMİKROBİYAL ÖZELLİKLERİ

Betül SARSIK

Karabük Üniversitesi
Lisansüstü Eğitim Enstitüsü
Biyomedikal Mühendisliği Anabilim Dalı

Tez Danışmanı:
Dr. Öğr. Üyesi Ammar Zeidan Ghailan ALSHEMARY
Temmuz 2021, 48 sayfa

Ortopedi ve travmatoloji ameliyatlarında kemik defektlerinin onarımı problem oluşturmaktadır. Kemik tedavilerinde biyomalzemelerin bakteriyel enfeksiyonları önlemesi ve kemik tedavisini daha erişilebilir hale getirmesi gerekmektedir.Bu çalışmanın ilk bölümünde β-trikalsiyum fosfat (βTCP) ve kobalt katkılı βTCP (Co-βTCP) malzemelerinin saf fazı mikrodalga destekli ıslak çökeltme yöntemi kullanılarak sentezlenmiştir. Hazırlanan tozlar, hem Co^{2+} katkısını doğrulamak hem de iyon katkılama üzerine yapısal ve moleküler özelliklerdeki değişiklikleri araştırmak için X-ışını Toz Kırınımı (XRD), Fourier-dönüşümlü kızılötesi spektroskopisi (FTIR) ve Taramalı elektron mikroskobu (SEM) teknikleri kullanılarak karakterize edildi. Co^{2+} iyonlarının dahil edilmesiyle, kafes parametreleri, kristallik derecesi ve βTCP'nin parçacık boyutu önemli ölçüde azaldı.

βTCP'nin (veya Co-βTCP) fonksiyonel grupları FTIR tekniği ile tespit edildi. βTCP'nin (veya CoβTCP) optik özellikleri, Ultraviyole ve görünür ışık spektrofotometri (UV–Vis) kullanılarak değerlendirildi. Co-βTCP malzemeleri için 530 ve 678 nm'de bulunan iki bant gözlendi. Bu çalışmanın ikinci bölümünde, su varlığında βTCP (veya Co-βTCP) ile monokalsiyum fosfat monohidrat (MCPM) arasında asit/baz reaksiyonu esas alınarak dikalsiyum fosfat (DCP) ve Co modifiye DCP (Co-DCP) kemik çimentoları üretilmiştir. Elde edilen kemik çimentoları XRD, FTIR ve SEM teknikleri kullanılarak karakterize edildi. DCP çimentoları bir monetit fazı olarak mevcuttu, monetit kristalinin a ve b ekseni Co^{2+} iyonlarının eklenmesiyle artarken, DCP yapısında artan Co^{2+} iyonları miktarı ile kristallik derecesi ve kristalit boyutu önemli ölçüde azaldı. DCP ve Co-DCP kemik çimentolarının *in vitro* bozunması, 37 ºC'de 14 gün boyunca fosfat tamponlu tuz çözeltisi (PBS) kullanılarak incelenmiştir. DCP kemik çimentolarının bozunması, Co^{2+} iyonlarının eklenmesiyle kontrol edildi. Saf ve Co katkılı DCP kemik çimentolarının antibakteriyel özellikleri, Escherichia coli (E. Coli), Metisiline duyarlı Staphylococcus aureus (MSSA)'ya karşı kalitatif olarak değerlendirildi. Metisiline dirençli Staphylococcus aureus (MRSA), Metisiline dirençli koagülaz negatif stafilokoklar (MR-CoNS) ve Pseudomonas aeruginosa (P. aeruginosa) bakterileri 37 ºC' de 24 saat süreyle bekletildi. Sonuçlar, Co^{2+} iyonlarının eklenmesiyle E.coli ve MSSA bakterilerinin büyümesini engellediğini gösterdi. Antibakteriyel özelliklere sahip hazırlanan kemik çimentoları, kemik onarımında enfeksiyona neden olan herhangi bir başarısızlığı önlemek için umut verici bir malzeme olacaktır.

Anahtar Kelimeler : Kemik çimentoları, Dikalsiyum fosfat, Kobalt, Karakterizasyonlar, Antibakteriyel özellikler

Bilim Kodu : 92503

ACKNOWLEDGMENT

My advisor, Assist. Prof. Dr. Ammar Zeidan Ghailan ALSHEMARY thanks for his help and support throughout my research. He shared his valuable information with me throughout the study.

I am also greatly obliged to Karabük University for providing financial support via Project no. KBÜBAP FYL-2020-2031. I would also like to my sincere thanks to Uzm. Dr. Murat Şahin and Assoc. Prof. Dr. Elçin KAL ÇAKMAKLIOĞULLARI for them help during this work.

I would like to thank all the teachers who contributed to me, especially my father as my first teacher.

To my family, who are the most valuable people I have, endless thanks for their support and love.

CONTENTS

Page

Page

Page

LIST OF FIGURES

Page

LIST OF TABLES

Page

SYMBOLS AND ABBREVITIONS INDEX

SYMBOLS

α : Alpha

β : Beta

Ag : Silver

Al : Aluminum

Ca : Calcium

Co : Cobalt

Cu : Copper

La : Lanthanum

Mg : Magnesium

P : Phosphorus

Sr : Strontium

Zn : Zinc

h : Hours

°C : Celcius

ABBREVITIONS

αTCP	: Alpha tricalcium phosphate
βTCP	: Beta tricalcium phosphate
MCPM	: Monocalcium phosphate monohydrate
DCP	: Dicalcium phosphate
PMMA	: Poly methyl methacrylate
UV-Vis	: Ultraviolet-visible spectroscopy
XRD	: X-Ray Diffraction
FTIR	: Fourier Transform Infrared Spectroscopy
ICP-OES	: Inductively Coupled Plasma - Optical Emission Spectrometry
SEM	: Scanning Electron Microscopy
CaP	: Calcium Phosphate
pH	: Power of Hydrogen
PBS	: Phosphate Buffer Saline
HA	: Hydroxyapatite
E.coli	: Escherichia coli
MSSA	: Methicillin-sensitive Staphylococcus aureus
MRSA	: Methicillin-resistant Staphylococcus aureus
MR-CoNS	: Methicillin-resistant coagulase negative staphylococci
ROS	: Reactive oxygen species
P. aeruginosa	: Pseudomonas aeruginosa

PART 1

INTRODUCTION

1.1. OVERVIEW

The number of bone fractures and osteoporosis are badly increased over the world. Different protocols have been applied to treat bone defects. Some of these methods are costly and may require extended time treatments. Bone cement is a well-known biomaterial used to fill the bone defects or binder between bone tissue and metallic implant.

The human bones are recognized as minerals reservoirs that gave the body shape and physically protecting the organs remaining inside the body [1]. The bones classified as cortical and spongy bones are based on the microstructure, as illustrated in Figure 1.1 [1]. Cortical bone contained 80% of bone mass, consisting of hydroxyapatite (HA), water, and collagen. It protects the inner space; it prevents bending and torsion. At the same time, the cancellous bone contained 20% of bone mass contains blood vessels and bone marrow. Bone cells are osteoblasts, osteocytes, and osteoclasts cells. Osteoblasts are cells that synthesize matrix proteins in cubic form and have the ability to form bone. Osteocytes are cells that keep bone tissue alive and transport substances. Osteoclasts are cells with resorption functions that destroy bone tissue. Osteoclasts destroy trabeculae or compact parts during bone formation, while osteoblasts produce new bone tissue [2]. In this way, new tissues come to replace the aging parts.

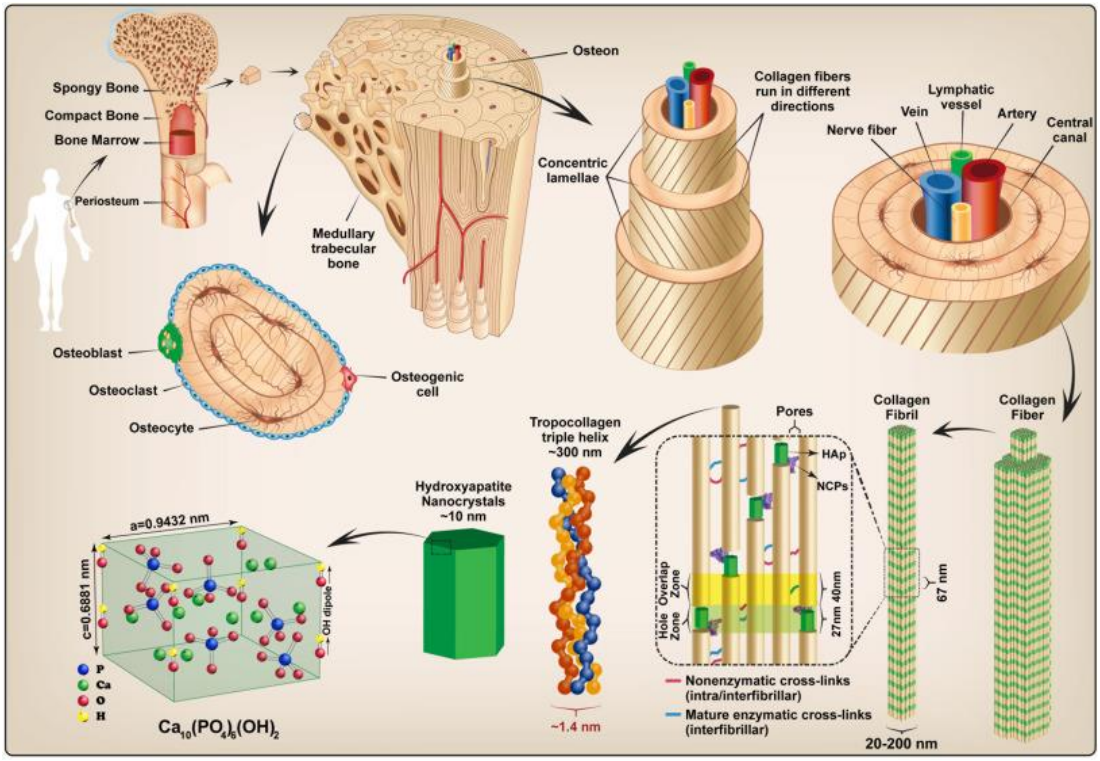

Figure 1.1. Ultrastructure of bone tissue [3].

Osteomyelitis is defined as inflammation of the bone and bone marrow (Figure 1.2). This disease can occur due to infectious agents, fungal or bacteria. In general, it is caused by bacteria [4]. Antibiotic treatment is applied to prevent bone death in the patient diagnosed with osteomyelitis. Osteomyelitis is difficult to treat because of the complex nature of the bone [5]. Conventional treatment methods require surgery and prolonged antibiotic therapy [6]. Surgeries often cause other bone defects that require further surgical intervention. High-dose and long-term antibiotic administration for the healing of the infected area may cause resistance and cause organ problems [7]. The amount and concentration of antibiotics used in long-term antibiotic treatments are insufficient to eliminate the infection as well as causing severe side effects [5]. In addition, intravenous antibiotic therapy requires a long hospital stay, which means high costs [6,8].

It is complicated to place ceramic implants with antibacterial properties in inaccessible parts of the bone. Surgical intervention in the infected area can lead to death or costly treatment [9]. Postoperative antibiotics cause toxicity in the surrounding tissues of the area where they are used [10]. Escherichia coli (E.coli),

Staphylococcus aureus (S. aureus), and pseudomonas aeruginosa (P. aeruginosa) are common bacteria that cause bacterial infection [8,11,12]. S. aureus is the most common antibiotic-resistant bacteria and causes permanent infection on implant materials [8]. The use of antibacterial ion-releasing biomaterials in antibiotic-resistant bacteria has been widely researched recently. Therefore, biomaterials need to provide controlled and continuous antibiotics to assist in infection stopping and support bone tissue [10].

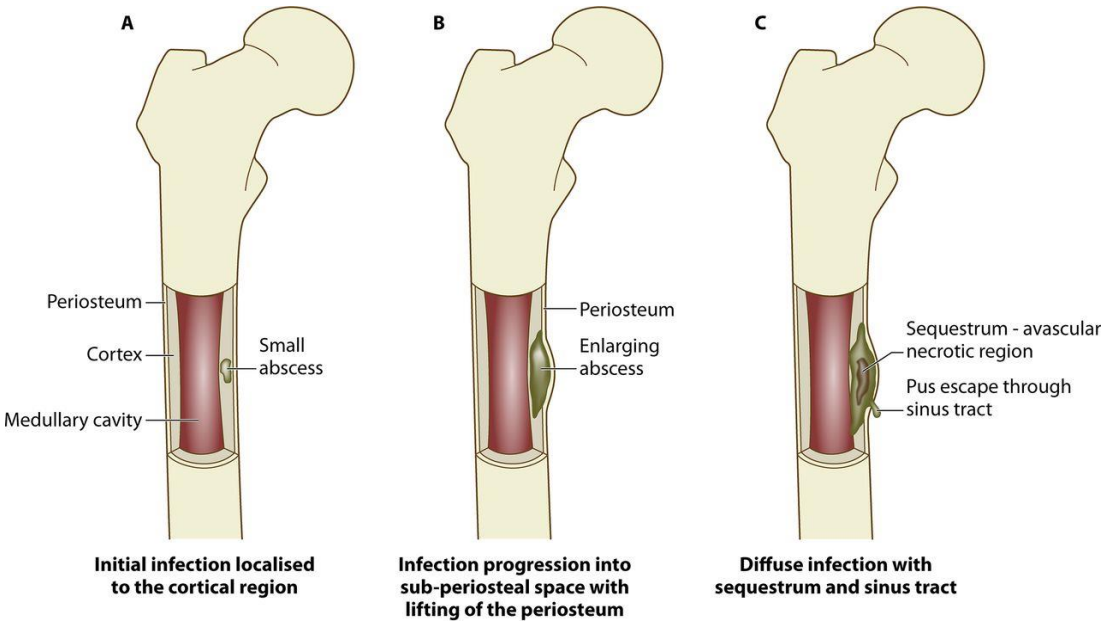

Figure 1.2. Progression of osteomyelitis [13].

Biomaterials used in place of tissues in the human body take a significant role in health. The biocompatibility, non-toxicity of these materials, response to the body, and no inflammation or infection in the body are very important. Similarly, orthopedic materials should be suitable for the human body. In selecting orthopedic materials, easy accessibility, reproducibility, shape ability, mechanical strength, biocompatibility, toxic effect, and corrosive effect are essential.

Bone cements are used in areas such as bone defects, bone injuries, and bone tumours. Bone cement is used together with the developing technology, and the healing process of the patients decreases. The bone cements are classified as

polymeric cement such as Poly (methyl methacrylate) (PMMA) and ceramic bone cement such as Dicalcium phosphate (DCP) cements based on their chemical nature.

PMMA is widely used as bone cement in joint replacement surgery, acted as a binder to bind metallic and polymer prostheses to the bone tissues; however, it has disadvantages are the exothermic polymerization reaction resulting in the formation of high temperatures, low biocompatibility, and release of unreacted monomers into the body and cause toxicity [14]. For that, the loading of antibiotics on the surface of PMMA will be difficult. In addition, PMMA bone cement exhibits shrinkage behaviour over time, creating a gap between the bone and the cement surface [14].

Recently, ceramic materials had a significant place in the biomedical discipline in the dental and orthopedic fields [15]. DCP bone cement attracts attention due to its high biocompatibility, osteoconductive, stability in the applied area, low risk of disease-carrying, and low cost [14]. It is self-setting at body temperature [16]. In the medical field, it is used in two forms: brushite and monetite. Studies showed that some metal ions have the ability to inhibit the growth of bacteria [17]. Furthermore, incorporation of metal ions into DCP cements structure may it will improve its antibacterial properties,

DCP bone cements containing Ag^{+}, Cu^{2+}, Zn^{2+} and Co^{2+} ions showed antibacterial properties [18,19]. Ag^{+} ions are known for their antibacterial, antifungal, and antiviral properties [11]. Ag^{+} ions show antibacterial properties on the cement surface. However, they do not show an antimicrobial effect on the tissues surrounding the cement [20]. Although Cu^{2+} ions are used in clinical applications due to their antibacterial properties, they have disadvantages such that they can rapidly return to the ionic state [17]. Zn^{2+} ions are preferred materials due to their antibacterial and antifungal properties and virus inactivation properties [19]. Although biomaterials secreting Zn^{2+} ions are used for treatment in clinical applications, they show a slow release that inhibits bacteria growth [19].

1.2. PROBLEM STATEMENTS

DCP bone cements are widely used in bone defects and bone repair in orthopedics and traumatology because they resemble bone structure. However, it has no antibacterial ability.

1.3. OBJECTIVES OF THE THESIS

The objectives of this thesis are:

- To synthesis and characterize pure βTCP and Co^{2+} ions doped βTCP materials.
- To evaluate the optical properties of pure βTCP and Co^{2+} ions doped βTCP bone cements.
- To synthesis and characterize pure DCP and Co^{2+} ions doped DCP bone cements.
- To estimate *in vitro* degradation rate of pure DCP and Co^{2+} ions doped DCP bone cements in PBS over 14 days.
- To evaluate the antibacterial properties of pure DCP and Co^{2+} ions doped DCP bone cements against Escherichia coli (*E. Coli*), Methicillin-sensitive Staphylococcus aureus (MSSA). Methicillin-resistant Staphylococcus aureus (MRSA), Methicillin-resistant coagulase negative staphylococci (MR-CoNS), and Pseudomonas aeruginosa (P. aeruginosa) bacteria.

1.4. SIGNIFICANT OF THE STUDY

Due to the low number of biomaterials in our country and the cost of biomaterials imported from other countries, the studies carried out in this thesis occupy an essential place for our country's economy and health technology.

PART 2

LITERATURE REVIEW

2.1. CALCIUM PHOSPHATES MATERIALS

Calcium Phosphates (CaP) materials are frequently used as bone substitution materials. Besides their bioactivity nature, CaP accelerates wound healing in body fluid [21]. βTCP and HA are the main phases of CaP materials. Poor antimicrobial properties are the main weak point of CaP [22]. For this reason, studies have been conducted in recent years to improve antibacterials properties of CaP materials and to produce more applicable bioceramics in the biomedical field.

2.1.1. Hydroxyapatite

HA [$Ca_{10}(PO_4)_6(OH)_2$] is an inorganic compound, resemble the mineral phase of human bone. HA is biocompatible and has high bioactivity nature; it is often preferred as bone substitution materials [23]. Furthermore, it's used as a scaffold material in the bone tissue regeneration process [24].

2.1.2. Monocalcium Phosphate Monohydrate

Monocalcium Phosphate Monohydrate [MCPM, $Ca(H_2PO_4)_2.H_2O$] belongs to the CaP materials family with a Ca/P ratio of 0.5. The crystal structure of MCPM is triclinic with a space group of P1 and unit-cell parameters of a=5.6261 Å; b=11.889; Å, c=6.4731 Å; α=98.633º, β=118.262º and γ= 83.344º [25]. Its high soluble material with

acidic nature, for that, it's used in previous studies as the main precursor of DCP bone cement, whereas it's mixed with a basic βTCP paste to obtain DCP after reaction [26].

2.1.3. β-tricalcium phosphate

βTCP [$Ca_3(PO_4)_2$) is a biodegradable ceramic widely used in the biomedical field. It could be used as bone filler or as bone scaffolds to improve the regeneration of bone tissue. Furthermore, it's considered the main precursor of DCP cements. Previous studies have been used as a femoral root coating in craniofacial defect repair and hip implants [27,28]. Furthermore, it helps the growth and differentiation of the cells, whereas the surface properties that provide adhesion of osteoblastic cells [29].

2.1.4. Doping of β-tricalcium phosphate

βTCP is defined as lattice rhombus (unit parameters: a = b = 10.43 Å, c = 37.39 Å, α = β = 90 °, γ = 120 °), as illustrated in Figure 2.1.

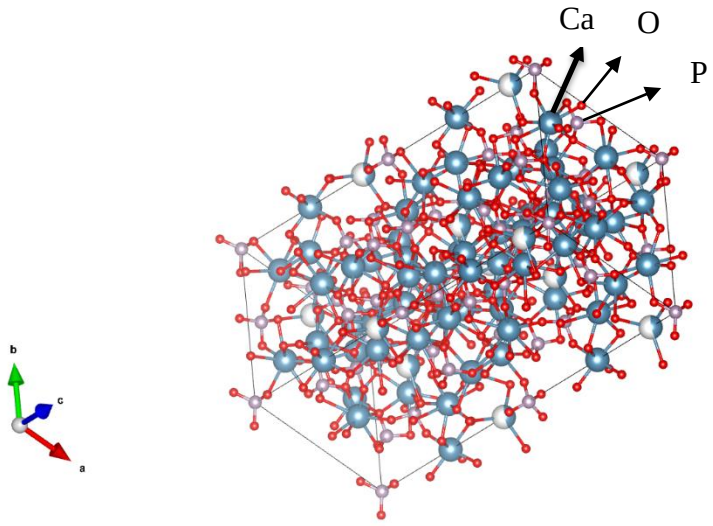

Figure 2.1. Crystal structure of βTCP.

Based on the chemical nature of βTCP, it has the ability to undergo ionic substitutions with different ions in Ca^{2+} and PO_4^{3-} sites. Various kinds and fractions

of ions have been added to the βTCP crystal lattice in order to enhance its physicochemical, mechanical, and biological properties.

2.1.4.1. Zinc Doped β-tricalcium phosphate

Along with CaP, the bone mineral contains many other inorganic elements. These elements played an important role in the mechanical and biological properties of human bone [30]. Zinc (Zn) is a metal needed for the activity of nucleic acid, protein synthesis and bone creation, bone development and wound healing [31]. Zn stimulates osseous creation and bone mineralization *in vivo* and *in vitro* environments [30]. Zn deficiency decreases bone intensity and flexibility, and this enhancement the risk of bone injury [32]. Furthermore, other studies demonstrated that zinc addition restricts postmenopausal bone loss [33].

Previous studies showed that the addition of Zn into CaP materials increases the bioactivity behaviour of the host [34]. Tas et al. observed that incorporating Zn into βTCP lattice enhances the growth of βTCP particles [33]. Araujo et al. found that substitution of Zn improves the optical properties of βTCP [35]. Zn oxides are very important in clinical applications due to their antibacterial, virus inactivation and antifungal activity properties [19].

2.1.4.2. Magnesium Doped β-tricalcium phosphate

Magnesium (Mg) is one of the ions that have a significant place in bone fragility and changes in the bone matrix [36]. Deficiency of Mg causes negative effects on skeletal metabolism, bone growth, and osteoblastic/osteoclastic cells activities [36].

Although Mg is preferred in biomedical applications due to its high biocompatibility and biodegradable properties, it has poor corrosion resistance [21]. Therefore, to use Mg-containing biomaterials in biomedical applications, the corrosion and degradation rate must be adjusted [21]. Furthermore, a study deduced that the addition of Mg ions increases the transition temperature of βTCP to α-tricalcium phosphate (αTCP) from 1180 °C to 1500 °C [37]. Zheng et al. found that the grain

size of βTCP gradually increased with Mg [38]. Banerjee et al. investigate the osteogenic ability of βTCP with binary incorporation of MgO/SrO, concluded that MgO/SrO co-doped βTCP they obtained supports the formation of new bone [39].

2.1.4.3. Silver Doped β-tricalcium phosphate

Bacterial infections caused or related to the implant position serious problems orthopedically [11]. Silver (Ag) has attracted the attention of researchers due to its antimicrobial activity and low toxicity [40]. It's well known that the Ag^+ ions have antimicrobial properties against a wide range of bacteria, fungi and some viruses [11].

Ewald et al., in their study, Ag^+ ions have found that it is possible to produce a fully absorbable bone replacement material, which reduces bacterial infections [40]. A study confirmed that the incorporation of Ag^+ ions improved the toughness and strength of CaP materials [41]. Matsumoto et al. concluded that substitution of Ag^+ ions enhanced antibacterials properties of βTCP [42]. Yuan et al. found that leaching of Ag^+ ions from Ag-doped βTCP materials contributed to the formation of new bone and repair of bone defects [43]. Gökçekaya et al. observed that the addition of Ag^+ ions enhanced the stability of the βTCP phase [44]. However, incorporation high of Ag^+ ions could show toxic behaviour [45].

There is various information about the antibacterial mechanism of Ag^+ ions in the literature. Ag^+ ions produced reactive oxygen species (ROS) by damaging bacteria's cell wall and entering the bacteria [46,47]. Ag^+ ions damaged the cytoplasmic contents of bacteria and destroyed vital enzymes [48]. It damaged vital functions by binding to important components of bacteria. It caused an osmotic collapse in the bacteria and released the substances inside the bacteria, causing the bacteria to die [49].

2.1.4.4. Cobalt doped β-tricalcium phosphate

Cobalt (Co) is a rare element required in mammals to form the B12 vitamin [50,51]. The human body contains 1.1-1.5 mg of Co, 43% in muscles, 14% in bones and the remainder in soft tissues [52,53]. A safe daily source of Co has been determined at a maximum of 0.012 μg [54]. A study confirmed that the Co^{2+} ions played an essential role in bone regeneration [55]. The doping of Co^{2+} ions is beneficial in healing osteoporosis-related bone defects and bone regeneration [56].

Wu et al. prepared Co^{2+} ions doped mesoporous bioactive glass scaffolds and found that the addition of Co^{2+} ions improved antibacterials of bioactive glass scaffolds against E.coli bacteria [57]. Kulanthaivel et al. evaluated the leaching profile of Co^{2+} ions over 60 days and found no toxic behaviour occurred [58]. The incorporation of Co^{2+} ions into HA lattice inhibited E. coli and S. aureus bacteria [53,54].

2.1.5. Synthesis methods of β-tricalcium phosphate

Different protocols have been used to synthesize βTCP particles, such as the sol-gel method, solid-state method, wet precipitation method and microwave-assisted wet precipitation method.

2.1.5.1. Sol-Gel Method

This method consists of hydrolysis, condensation, gelation, aging, drying and densification [59]. Calcium nitrate tetrahydrate ($Ca(NO_3)_2 \cdot 4H_2O$), citric acid monohydrate ($C_6H_8O_7 \cdot H_2O$), and diammonium phosphate ($(NH_4)2HPO_4$) and the ion source to be doped are used to produce doped- βTCP by the sol-gel method [60]. The amount to be used is determined by calculating (Ca + doped ion) / P = 1.5 molar ratio. After the chemical materials are mixed in a magnetic stirrer, a gelatinous structure is expected to form. The gelatinous structure, which is dried at 180 degrees for 12 h, is then calcined at 1000 °C for 3 h [61].

It shows good physical and chemical properties [61]. However, a long preparation time could be a weak point [62]. If the drying process is not done too slowly and carefully, the gel mesh could be damaged [63].

2.1.5.2. Solid State Method

βTCP was prepared by solid-state reaction of Calcium carbonate ($CaCO_3$) combined with brushite in the molar ratio of 1:2 at 1000 °C for 12 h [64]. Although better quality powder can be produced in this method, it is not preferred because it's required a high temperature in the production stage [65].

2.1.5.3. Wet Precipitation Method

Calcium nitrate tetrahydrate and diammonium hydrogen phosphate were used as a source of Ca^{2+} and PO_4^{3-} ions. They are mixed at a ratio of Ca/P=1.5 [8]. The speed of this process may vary due to reasons such as reaction temperature, pH of the solution, concentrations of starting salts, and residence time [66]. The precipitate was collected on a filter and washed with water, dried at 80-100 °C, calcined at 700-800 °C [67]. Furthermore, other studies could be calcined at a lower degree [32]. However, this method takes a long time to prepare the βTCP which is considered as a weakness point [62].

2.1.5.4. Microwave-Assisted Wet Precipitation Method

Calcium nitrate tetrahydrate and diammonium hydrogen phosphate were dissolved in distilled water for 30 minutes in a magnetic stirrer to obtain βTCP by microwave-assisted wet precipitation method [68,69]. Ammonium hydroxide was slowly added to pH 7 and then the solution was transferred to the microwave attached to the reflux system [69]. The precipitation irradiated for 5 minutes in the microwave at 800 W. The precipitation was collected and washed with distilled water then dried at 80 °C for 24 h [68,70]. The final product was calcined at 1000 °C for 2 h [70].

Microwave irradiation is used in this method after mixing the solutions to ensure fast precipitation [71]. Microwaves in this method are simple, quick (40-45 minutes), and effective compared to traditional methods [72]. While ordinary heating methods provide superficial heating, microwave heating provides volumetric heating. Microwave heating is cheap, non-polluting, and allows the production of CaP particles with smaller particle sizes [73].

2.2. DICALCIUM PHOSPHATE CEMENTS

DCP bone cements are biocompatible, bioactive, osteoconductive, injectable and mouldable [74]. It's compatible with living tissues and showed no toxic or harmful effect. For that, it's frequently used as bone filler and considered as a source of Ca^{2+} and PO_4^{3-} ions which contributed to the bone healing process [75]. Furthermore, its self-Harding at body temperature, injectability, excellent results on implant sites [76]. Usually, there are two main phases for the DCP cement, namely brushite and monetite.

Brushite and monetite cement have recently attracted attention due to their metastasis under physiological conditions, bone regeneration success, and rapid absorption. Scientists think this is the pioneer of bone mineralization [77]. DCP cements are difficult to use and do not show antimicrobial activity. For this reason, many studies are carried out to increase the properties of DCP cements.

2.2.1. Brushite

Brushite ($CaHPO_4 \cdot 2H_2O$) cements are used in the biomedical field to form new bone, repair cranial defects, maxillofacial bone, and periodontal treatments [66,78,79]. βTCP materials are used as the main precursors for brushite cement. It is formed by the combination of βTCP and MCPM, provides higher set times and a high level of resorbability. It is used in biomedical applications where it is desired to replace bone due to chemical degradation [80]. Brushite cements have a short adjustment time, a strategy of increasing the liquid powder ratio or adding a molecule that provides a delay of the adjustment process is applied [81].

2.2.2. Monetite

Monetite ($CaHPO_4$) is very rare in nature and non-toxic materials. In the biomedical field, it can be used as a single-phase or together with other CaP phases. Monetite is an excellent alternative to bone graft or porous matrix for use in bone tissue engineering [81]. In rabbit experiments, monetite granules showed osteoconductive properties in cranial defects, and their longtime *in vivo* achievement was superior to other CaP materials like brushite and HA [82]. Due to its osteoconductive and resorbable properties, monetite is more soluble than brushite and therefore, it's frequently used in tissue engineering [83]. In orthopedic and dental fields, monetite is used as injectable bone cement and biodegradable bone scaffold [84,85]. Based on its chemical nature, the monetite has no antimicrobial properties.

Various methods have been used to synthesis the monetite, such as Sonochemical, Wet precipitation, Hydrothermal, and Thermal conversion methods [86].

2.2.2.1. Doping of Monetite

The monetite unit cell parameters are as follows: a = 6.910, b = 6.627, c = 6.998 Å, α = 96.34°, β = 103.82°, γ = 88.33° [87]. Monetite has a triclinic structure (Figure 2.2.)

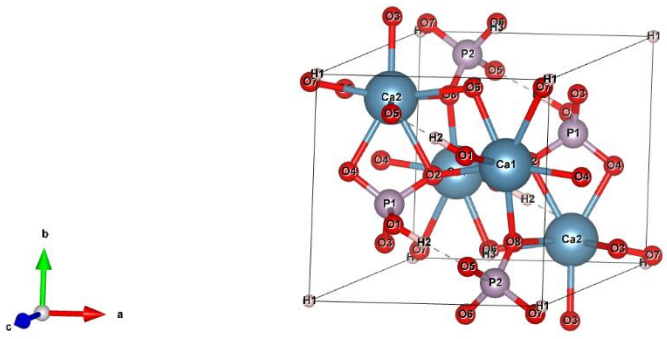

Figure 2. 2 Crystal structure of monetite.

Many researchers included different foreign ions into the DCP cements structure to improve physicochemical, mechanical, antibacterials, and biological properties of DCP cements. The studies were summarized in Table 2.1.

Table 2. 1. Impact of dopants on the properties of DCP cements.

COMPOSITION	DOPANTS	NOTES	REF
Brushite	0.25-1.00 gm of Mg^{2+} ions	With the incorporation of Mg^{2+} ions: • The setting time was increased from 2 minutes to 33 minutes. • The injectability rose from 10% to 77%. • The compressive strength increased from 1.323 MPa to 20.98 MPa.	[88]
Brushite	26.67-66.67% of Mg^{2+} ions	With the incorporation of Mg^{2+} ions: • The porosity is decreased. • Inhibited growth of S. aureus bacteria.	[89]
Brushite	6.67-66.67% of Mg^{2+} ions	With the incorporation of Mg^{2+} ions: • The setting time was increased from 20 minutes to 90 minutes. • No changes in the tensile strength of cement were observed.	[90]
Brushite	0.6-1.0 wt. % of Ag^{+}	With the incorporation of Ag^{+} ions: • The compressive strength of cement was decreased from 6.5 ± 1.0 MPa to 1.5 ± 1.0 MPa • Inhibited growth of E. coli bacteria.	[91]
Brushite	1.0 mole of Ag^{+} ions	With the incorporation of Ag^{+} ions: • The compressive strength of cements was increased by 30%. • Inhibited S. aureus and S. epidermidis bacteria.	[40]
Brushite	0.25 wt.% of	With the incorporation of Zn^{2+} ions:	[92]

COMPOSITION	DOPANTS	NOTES	REF
	Zn^{2+} ions	• The compressive strength of cements was decreased from 4.78 ± 0.21 to 3.78 ± 0.59 • The setting time was increased from 11 minutes to 19 minutes.	
Brushite	0.6-1.2 wt.% of Zn^{2+} ions	With the incorporation of Zn^{2+} ions: • The setting time was increased from 7 minutes to 19 minutes. • Inhibited growth of E. coli bacteria.	[93]
Brushite	2.4-8.9 wt.% of Sr^{2+} ions	With the incorporation of Sr^{2+} ions: • The setting time was increased from 5 minutes to 25 minutes. • The injectability was increased from 10% to 66%.	[94]
Brushite	0.25-1.0 wt.% of Co^{2+} ions	With the incorporation of Co^{2+} ions: • The setting time was increased.	[95]
Brushite	0.3-1.2 wt.% of Co^{2+} ions	With the incorporation of Co^{2+} ions: • The compressive strength of cement was decreased from 3.17 ± 1.04 MPa to 2.11 ± 0.33 MPa. • The setting time of cement was increased from 3.67 ± 0.23 minutes to 6.80 ± 0.08 minutes.	[96]

COMPOSITION	DOPANTS	NOTES	REFs
Monetite	0.25-1.0 mole of Sr^{2+} ions	With the incorporation of Sr^{2+} ions: • The injectability of cements was increased from 10% to 45%. • The setting time of cements was decreased from 5 minutes to 17 minutes	[94]
Monetite	0.01-0.294 mole of Ag^{+} ions	With the incorporation of Ag^{+} ions: • Inhibited growth of S. epidermis bacteria.	[97]
Monetite	0.09-0.45 mole of La^{3+} ions	With the incorporation of La^{3+} ions: • The lattice parameters of the crystal structure were increased. • The setting time of cements was decreased from 42 minutes to 20 minutes.	[98]
Monetite	1-24 wt.% of Zn^{2+} ions	With the incorporation of Zn^{2+} ions: • Reduced the total porosity. • Improved cell proliferation.	[99]

REFs= References.

PART 3

METHODOLOGY

3.1. MATERIALS

Di-ammonium hydrogen phosphate ($(NH_4)_2HPO_4$) (Merck-Germany), Calcium nitrate tetrahydrate ($Ca(NO_3)_2.4H_2O$) (Merck-Germany), and Cobalt(II) nitrate hexahydrate ($Co(NO_3)_2 \cdot 6H_2O$) (Merck-Germany) were used as precursors to prepare pure βTCP and Co^{2+} doped βTCP materials. Ammonia solution 25% (NH_4OH) (Merck-Germany) was used to adjust the pH value. Monocalcium phosphate (MCPM) ($Ca(H_2PO_4)_2$) (Merck-Germany) was used as a precursor to prepare monetite cement. Sodium chloride (NaCl) (Merck-Germany), Potassium chloride (KCl) (Merck-Germany), Sodium hydrogen phosphate (Na_2HPO_4) (Merck-Germany), Potassium dihydrogen phosphate (KH_2PO_4) (Merck-Germany) were used to prepare Phosphate-buffered saline (PBS) solution.

3.2. PREPARATION OF PURE βTCP AND CO^{2+} IONS DOPED βTCP

About 15.85 g of $(NH_4)_2HPO_4$ dissolved in 200 mL of distilled water (solution A), and approximately 42.51 g of $Ca(NO_3)_2.4H_2O$ was dissolved in 200 mL of distilled water (solution A). Solution A added dropwise to solution B under stirring for 30 minutes, and the pH value was adjusted to 7 using NH_4OH. The white precipitation was transferred to Microwave (ARÇELİK MD 500) attached to the refluxing system and irradiated for 5 minutes. The white precipitation was collected and washed and filtered, and dried in an oven at 80 ºC for 24 h. The dried powder was calcined using a furnace at 1000 ºC for 2h.

Co^{2+} ions doped βTCP materials were prepared using the same protocol with a different additional amount of Co $(NO_3)_2 \cdot 6H_2O$. as described in Table 3.1.

Table 3. 1. Nominal compositions of pure βTCP and Co^{2+} ions doped βTCP.

	REACTANTS		
SAMPLE ID	**CALCIUM (G)**	**PHOSPHATE (G)**	**COBALT (G)**
βTCP	42.51 g	15.85 g	-
1Co- βTCP	42.08 g	15.85 g	0.78 g
2Co- βTCP	41.44 g	15.85 g	1.31 g
3Co- βTCP	40.38 g	15.85 g	2.62 g

3.3. SYNTHESIS OF MONETITE CEMENT

About 1 g of βTCP (or Co-βTCP) mixed thoroughly with 0.5 g of MCPM till gain homogenised powder. About 0.8 ml of distilled water was added to the mixed powder and crushed using mortar and pestle to get a homogenized paste. Then, the paste was cast using Teflon moulds (10 mm) and carefully removed from the moulds with the help of iron bars. The discs are allowed to dry for 1-2 days.

3.4. CHARACTERIZATION

To evaluate the physicochemical properties of the prepared materials, different techniques have been used, such as:

3.4.1 X-Ray Diffraction

The phase purity, degree of crystallinity, and lattice parameters of the prepared powders were estimated using X-Ray Diffraction (XRD, MODLE Rigaku Ultima IV) technique. The diffraction patterns were taken for the 2θ range of 10° to 80° with a step of 0.03°.

3.4.2. Scanning Electron Microscopy

The particles shape, particles size, and elemental mapping of the prepared materials were visualized using Scanning Electron Microscopy (ZEISS ULTRA PLUS SEM). Samples were pre-coated with a gold thin film to reduce the spark rate. Particles distributions were evaluated using ImageJ software.

3.4.3. Fourier Transform Infrared Spectroscopy

The vibration bands of functional groups in the prepared materials were identified using Fourier transform infrared spectroscopy (FTIR, Bruker IFS 66/S). The data received at room temperature were recorded by scanning in the wavelength range of 4000 - 400 cm^{-1}.

3.4.4. Diffuse Reflectance UV-Vis Spectroscopy

The absorption spectra of Co^{2+} doped DCP cement was measured using a UV-Vis spectrophotometer (Perkin Elmer Lambda 35 UV-Vis Spectrophotometer). The absorption spectra were taken in the range of 200-800 nm.

3.5. *IN VITRO* DEGRADATION

The degradation rate of pure and Co doped DCP cement was evaluated using PBS. The discs (dimension and wt) were immersed in 50 mL PBS (pH 7.4) at 37 ºC for 1, 3,7 and 14 days. At each set period, the discs were gently removed, and the filtrates were collected. The leaching profiles of Ca^{+}, PO_4^{3-} and Co^{2+} ions in PBS media were detected using Inductively Coupled Plasma – Optical Emission Spectrometry (ICP-OES). The experiments were performed in triplicates.

3.6. *IN VITRO* ANTIMICROBIAL ACTIVITY

Antibacterial properties of pure and Co doped DCP cement were evaluated qualitatively against Escherichia coli (E. Coli) (gram(-)), Methicillin-sensitive

Staphylococcus aureus (MSSA) (gram(+)), Methicillin-resistant Staphylococcus aureus (MRSA) (gram(+)), Methicillin-resistant coagulase negative staphylococci (MR-CoNS) (gram(+)), and Pseudomonas aeruginosa (P. aeruginosa) (gram(-)) bacteria. Qualitative assessment was conducted out via the disc diffusion method. The discs were gently placed on the inoculated plates and were incubated at 37 ºC for 24 h.

PART 4

RESULTS AND DISCUSSION

4.1. CHARACTERIZATION OF PURE βTCP AND Co-βTCP POWDERS

The phase purity and crystallinity of pure βTCP and Co-βTCP samples sintered at 1000 °C for 2 h were illustrated in Figure 4.1.

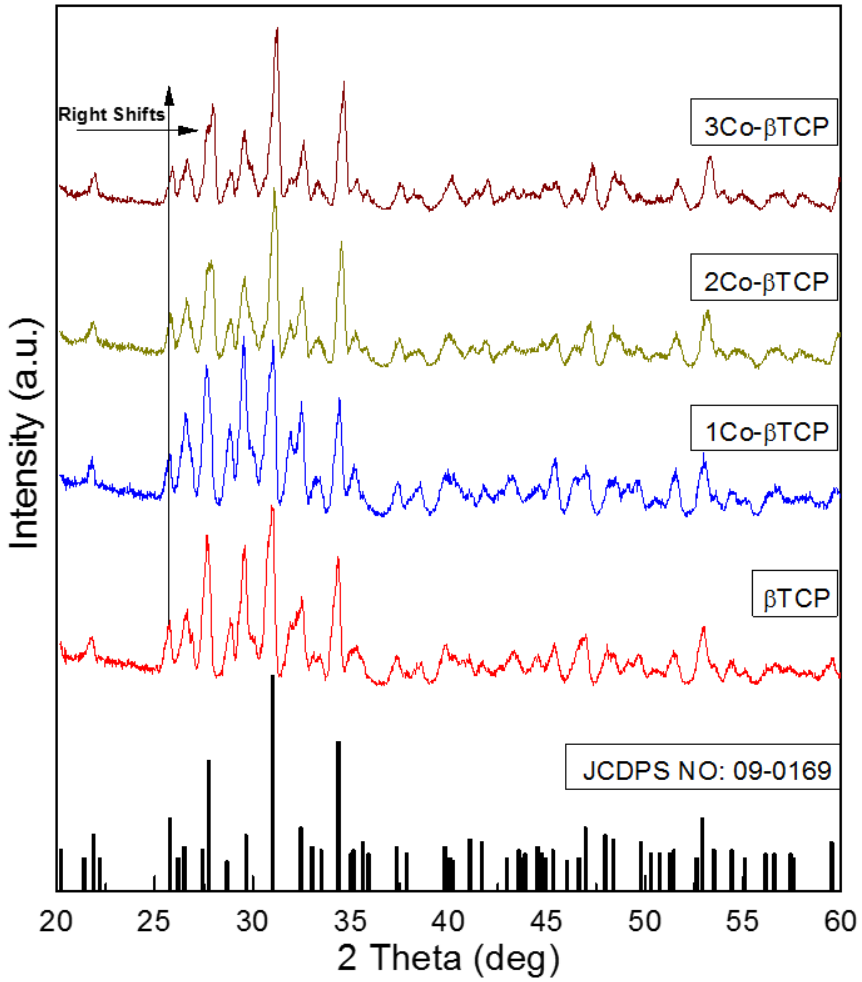

Figure 4.1. XRD patterns of βTCP and Co-doped βTCP materials were calcined at 1000 °C for 2 h.

XRD pattern of pure βTCP was in harmony with the standard phase of βTCP (JCDPS NO: 09-0169). No other CaP phases were observed. However, a slight reduction in lattice parameters along with *a* and *b* axis was observed (Table 4.1), and this reduction could be attributed to local changes in the bond length [100]. With the incorporation of Co^{2+} ions, some changes were observed with diffraction peaks of βTCP. The diffraction planes of βTCP were shifted to the higher value of 2 thetas which could be attributed to shrinkage in lattice parameters (Table 4.1). This behaviour could be attributed to the substituted smaller ionic size of Co^{2+} ions (0.074 nm) with the larger ionic size of Ca^{2+} ions (0.099 nm). Tank et al. and Pang et al. found that the diffraction peaks of HA shifted to the high value of 2 thetas with the incorporation of Co^{2+} ions, causing reducing unit-cell parameters [101,102]. Furthermore, Pang et al. observed that not all amounts of Co^{2+} ions substituted into HA structure, a part of Co^{2+} ions existed on the surface of HA in the shape of Cobalt tetraoxide (Co_3O_4) [102]. While, in the obtained results, no peaks were detected at 36.85°, confirmed that the Co_3O_4 was absent, indicating that all Co^{2+} amount was incorporated into HA lattice. Furthermore, the intensity or sharpness of diffraction peaks was gradually decreased, and width gradually increased with substitution of Co^{2+} ions, demonstrating a reduction in the degree of crystallinity and crystallite size (Table 4.1), respectively.

Table 4. 1. Lattice parameters, degree of crystallinity and crystallite size of XRD pure βTCP and Co doped βTCP powders.

ID	**LATTICE PARAMETERS**				**DC(%)**	**ACS (nm)**
	a(Å)	**b(Å)**	**c(Å)**	**CV(Å)^3**		
Std. βTCP	10.429	10.429	37.38	3520.9	----	----
βTCP	10.401	10.401	37.30	3520.9	89.56	16.52
1Co-βTCP	10.380	10.380	37.37	3506.9	84.37	15.73
2Co-βTCP	10.353	10.353	37.24	3463.7	75.87	13.84
3Co-βTCP	10.323	10.323	37.23	3448.4	57.81	15.28

CV= Cell Volume, DC= Degree of Crystallinity, ACS= Average crystallite size.

The functional groups of pure βTCP and Co-βTCP powders sintered at 1000 °C for 2h were illustrated in Figure 4.2.

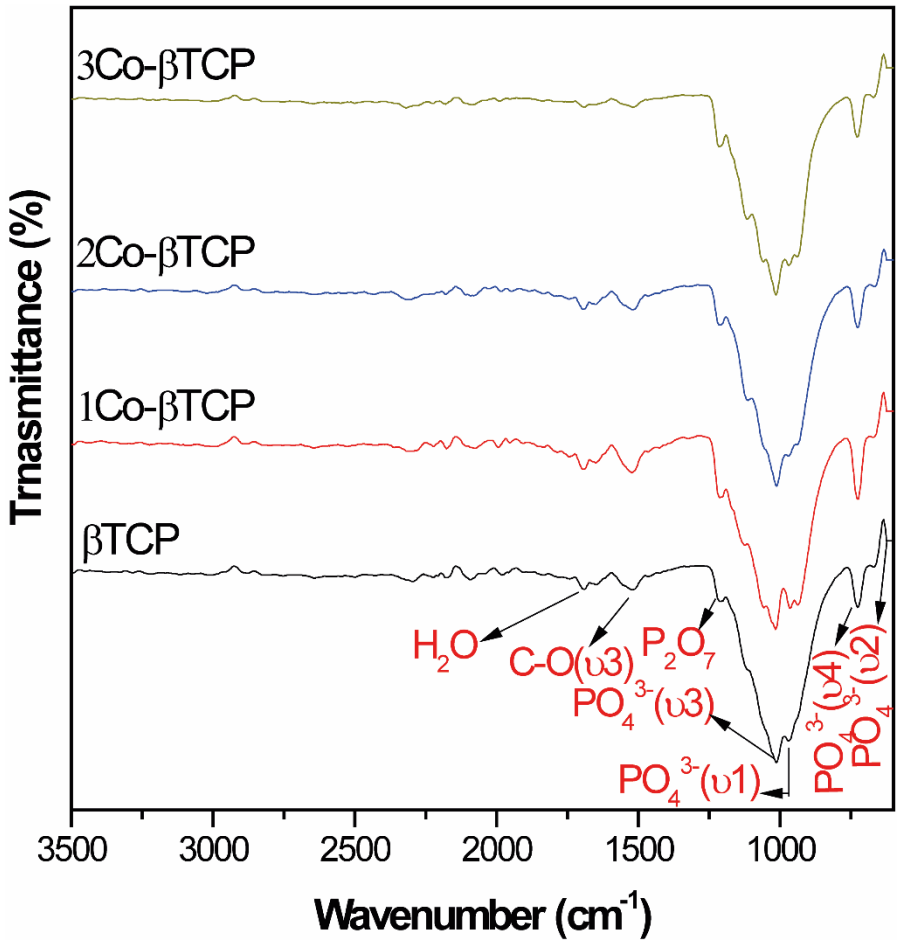

Figure 4.2. FTIR spectrum of pure βTCP and Co-βTCP powders.

The prominent characteristic bands of βTCP appeared in Figure 4.2. The bands located at 630, 725, 970, and 1013 cm^{-1} belonged to the vibration mode of (υ2) PO_4^{3-}, (υ4) PO_4^{3-}, (υ1) PO_4^{3-}, and (υ3) PO_4^{3-}, respectively. A tiny spectra was detected at 1215 cm^{-1} could be assigned to the vibration mode of P_2O_7. The small bands observed at 1535 and 1694 cm-1 were attributed to the stretching mode of (υ3) CO_3^{2-} groups and the vibration mode of absorbed H_2O molecules. The location of functional groups observed in the spectra of the pure phase of βTCP were in good match with a wide range of previous studies [94,97].

With the incorporation of Co^{2+} ions into βTCP lattice, it can be seen that (i) There are no changes in the location of bands, (ii) The intensity of bands was diminished gradually upon the increasing amount of Co^{2+} ions, which could be assigned to the reduction in the degree of crystallinity, as calculated and approved in Table 4.1, (iii) The peaks area were expanded with the addition of Co^{2+} ions, which could be attributed to the incorporation of Co^{2+} ions into βTCP crystal structure. Robles-Aguila et al. found that the substitution of Co^{2+} ions into HA resulted in an expansion in the spectra area of (υ3) PO_4^{3-} [103]. Girase et al.. evaluated the impact of Co^{2+} ions doping on the FTIR spectra of lead iodate crystals, found that incorporation of Co^{2+} ions leads to a minor shift in the band spectra, which could be ascribed to the differences in the mass number of a wavenumber may be due to the difference in mass number of Co^{2+} ions with the host system [104].

The micrograph images and particle distributions of pure βTCP and Co-βTCP powders were displayed in Figure 4.3(a-d). The images of pure βTCP existed in the spheroid agglomeration shape and were well distributed. The particles appeared coalescence, which could be due to heat treatment at high temperatures [105]. The average diameter of βTCP particles was about 300 nm. Puroniene et al. synthesized pure phase of βTCP particles using the wet precipitation method and calcined them at 800 ºC. The size of the obtained particles was in the range of 100-300 nm [105]. With the addition of Co^{2+} ions, no significant changes in the shape of particles were observed. However, the particles became more homogeneous and more interconnected nature. Numerous small spherical particles were observed on the surface of the grains. Since the crystals do not have a particular direction to show, there is a possibility that there may be more or less isotropic behaviour [106]. Furthermore, the diameter of βTCP particles decreased from 300 nm to 246 nm for (3Co-βTCP). Stojanović et al. demonstrated that the addition of 4.3 at% of Co^{2+} ions provoked the average size of HA from 94 to 63 nm[26]. The crystallite size of βTCP and Co- βTCP were significantly lower than particles size (Table 4.1). This behaviour could be due to aggregates in the particle-size analyzed particles, consisting of several crystallites[26].

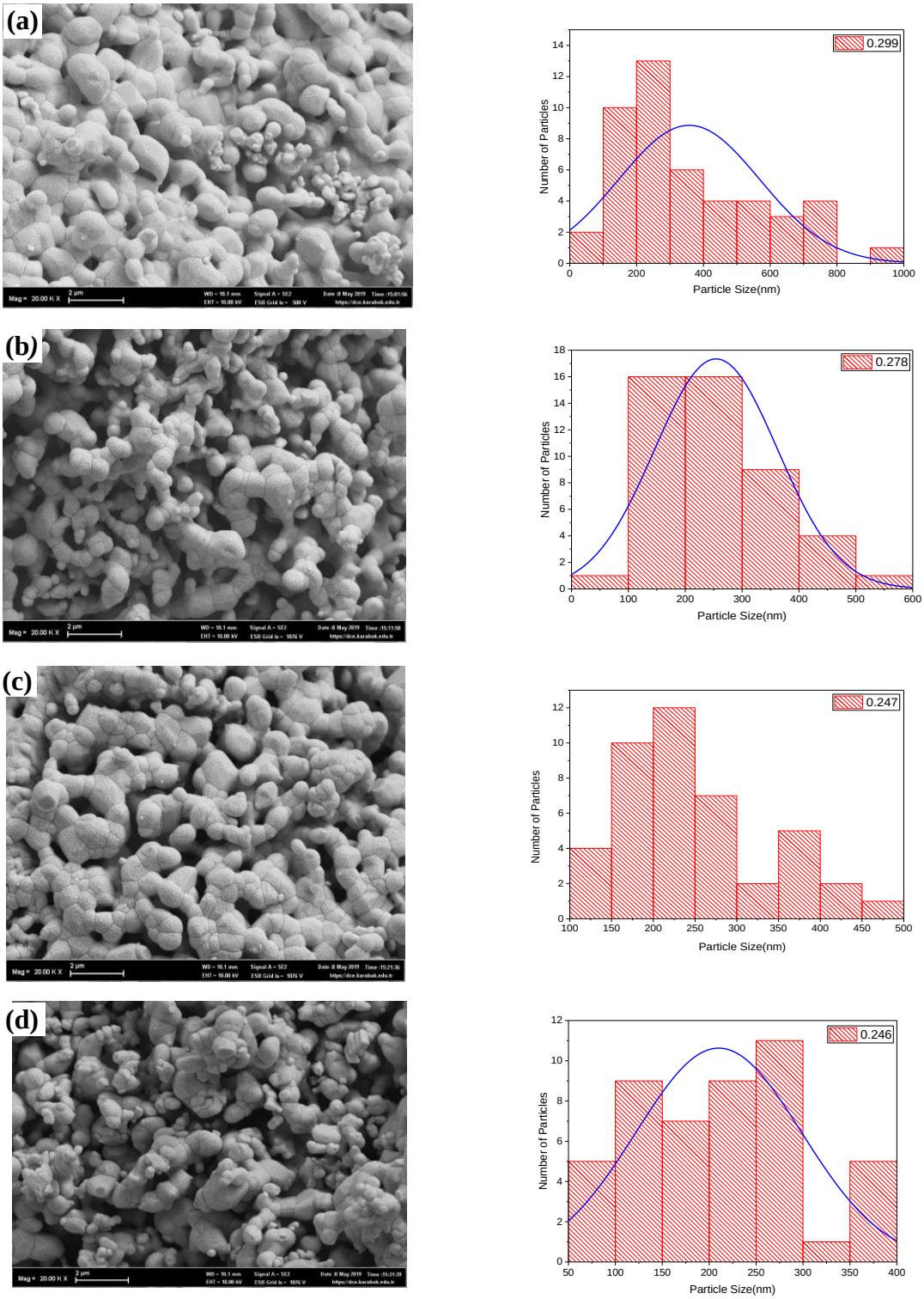

Figure 4. 3. SEM images and particle distributions of pure βTCP (a), 1Co- βTCP (b), 2Co- βTCP (c), and 3Co- βTCP (d).

Optical imaging techniques are used in biomedical research and the healthcare industry for diagnosis. It is used in daily clinical practice, oxygen saturation

measurement, cancer diagnosis, and tumour therapy [107,108]. While obtaining diagnostic information from light-tissue interaction thanks to optical imaging, it is preferred because of its advantages such as ease during diagnosis, sensitivity, providing high resolution, non-invasive, clearer display of biological components, and allowing real-time monitoring [106,109]. The UV-Vis absorption spectra of βTCP and Co doped
βTCP particles are shown in Figure 4.4.

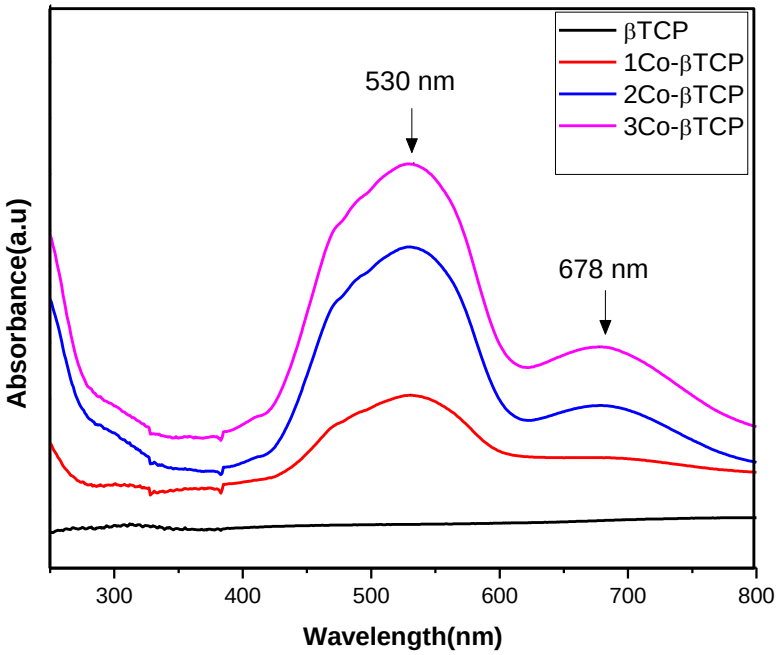

Figure 4. 4. UV-Vis absorption spectra of βTCP and Co doped βTCP powders.

The βTCP materials synthesized in our lab existed as white powders, while with the incorporation of Co^{2+} ions, the colour turn into pink colour, the intensity of colour increased upon the increasing amount of Co^{2+} ions. For the pure phase of βTCP, no absorption band has been detected. UV-Vis spectra were significantly enhanced with the substitution of Co^{2+} ions. Two peaks appeared with the incorporation of Co^{2+} ions. The first broad peak was located at 530 nm. The peak was existed due to the $^4T_{1g}$ to $^4T_{1g}(P)$ transition [110]. The other peak was detected at 678, assigned to $^4T_{1g}$ to $^4A_{2g}$ transition [110].

4.2. CHARACTERIZATION OF PURE DCP AND Co-DCP BONE CEMENTS

The phase identification of pure DCP and Co doepd DCP cements set at the lab temperature was achieved, and the results are shown in Figure 4.5.

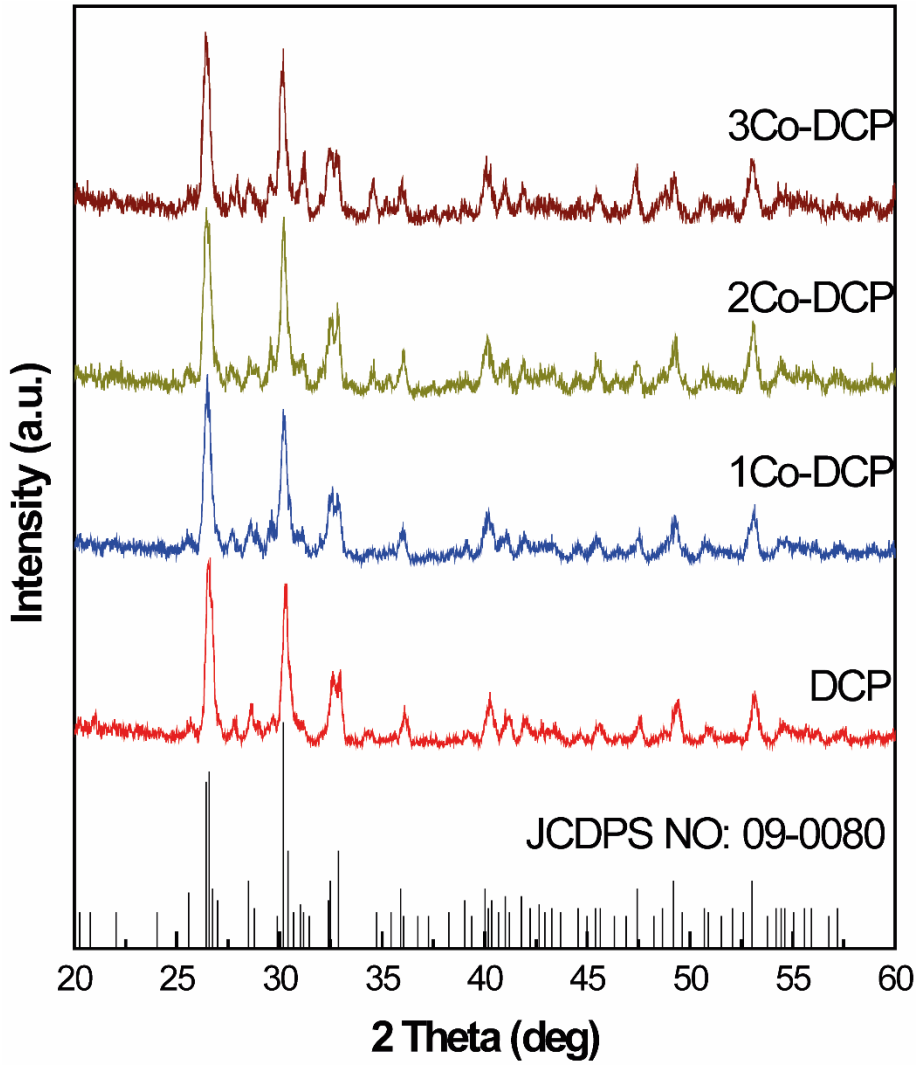

Figure 4.5. XRD patterns of DCP and Co-doped DCP cements set at the lab temperature.

The diffraction peaks of all samples were in good match with the standard phase of monetite (JCDPS NO: 09-0080). No peaks were observed at 11.5º and 23.31º, indicating that the prepared cements were free of brushite phase (JCDPS NO: 11-0293). Variations in the DCP (monetite phase) lattice parameters compared to the

standard phase of monetite were observed (Table 4.2.). The XRD patterns of Co doped DCP cements show crystalline phase with expansion along with a,b axis, and reduction along with c axis. Furthermore, crystallinity and crystallite size significantly decreased with the increasing amount of Co^{2+} ions into the DCP structure. This behaviour could be attributed to substituting bigger sized Ca^{2+} ions with smaller sized Co^{2+} ions in the DCP lattice.

Table 4. 2. Lattice parameters, degree of crystallinity and crystallite size of pure DCP and Co doped DCP cements.

ID	**LATTICE PARAMETERS**				**DC(%)**	**ACS (nm)**
	a(Å)	**b(Å)**	**c(Å)**	**CV(Å)^3**		
Std. Monetite	6.906	8.577	6.634	309.4	----	----
DCP	6.883	8.593	6.643	310.0	70 %	20.1 nm
1Co-DCP	6.885	8.560	6.636	308.4	67.69%	15.25 nm
2Co-DCP	6.888	8.568	6.634	309.0	67.24%	15.06 nm
3Co-DCP	6.913	8.572	6.633	309.1	64.83%	12.5 nm

The functional group present in the pure DCP and Co^{2+} doped DCP cements were evaluated using FTIR spectra, and the results are displayed in Figure 4.6.

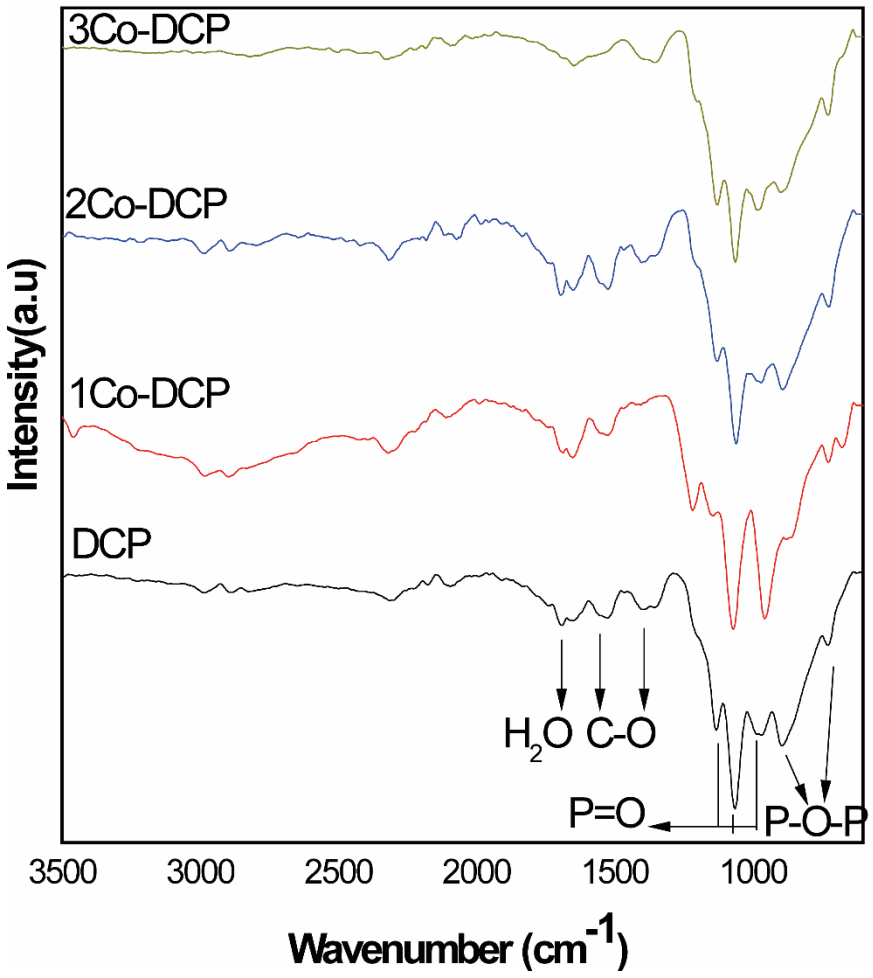

Figure 4. 6. FTIR spectra of pure DCP and Co doped DCP cements.

The stretching mode of P-O-P and P=O bonds appeared, the stretching mode of C-O existed in two locations, and the bending mode of O-H was also detected in the pure DCP sample. With the addition of Co^{2+} ions into the DCP structure, no significant changes were observed in the location of bands (Table 4.3.).

Table 4.3. Characteristic peaks of pure DCP and Co doped DCP cements in the FTIR spectrum

FTIR PEAKS (cm^{-1})				
DCP	**1Co-DCP**	**2Co-DCP**	**3Co-DCP**	**VIBRATIONAL MODE**
727	727	727	727	asymmetric stretching vibrations P-O-P
888	856	888	888	asymmetric stretching vibrations P-O-P
974	952	974	974	stretching mode of P=O
1059	1070	1059	1059	stretching mode of P=O
1123	1145	1123	1123	stretching mode of P=O
1392	---	1392	1402	stretching mode of C-O
1530	1530	1510	1520	stretching mode of C-O
1659	1659	1670	1638	bending mode of O-H

SEM micrograph images of pure DCP and Co doped DCP bone cements are presented in Figure 4.7. SEM of pure DCP revealed the formation of small structured particles of irregular shape (Figure 4.7(a)), which switched to the loosely packed plate-like morphology with heterogeneous size distribution upon Co^{2+} doping (Figure 4.7(b-d)). The plates did not reveal a particular orientation, indicating a more or less isotropic behaviour [7]. Successful homogenous substitution of Co^{2+} ions into the DCP bone cements was further verified by the elemental mapping of Ca, P, Co, and O elements utilizing SEM (Figure 4.7).

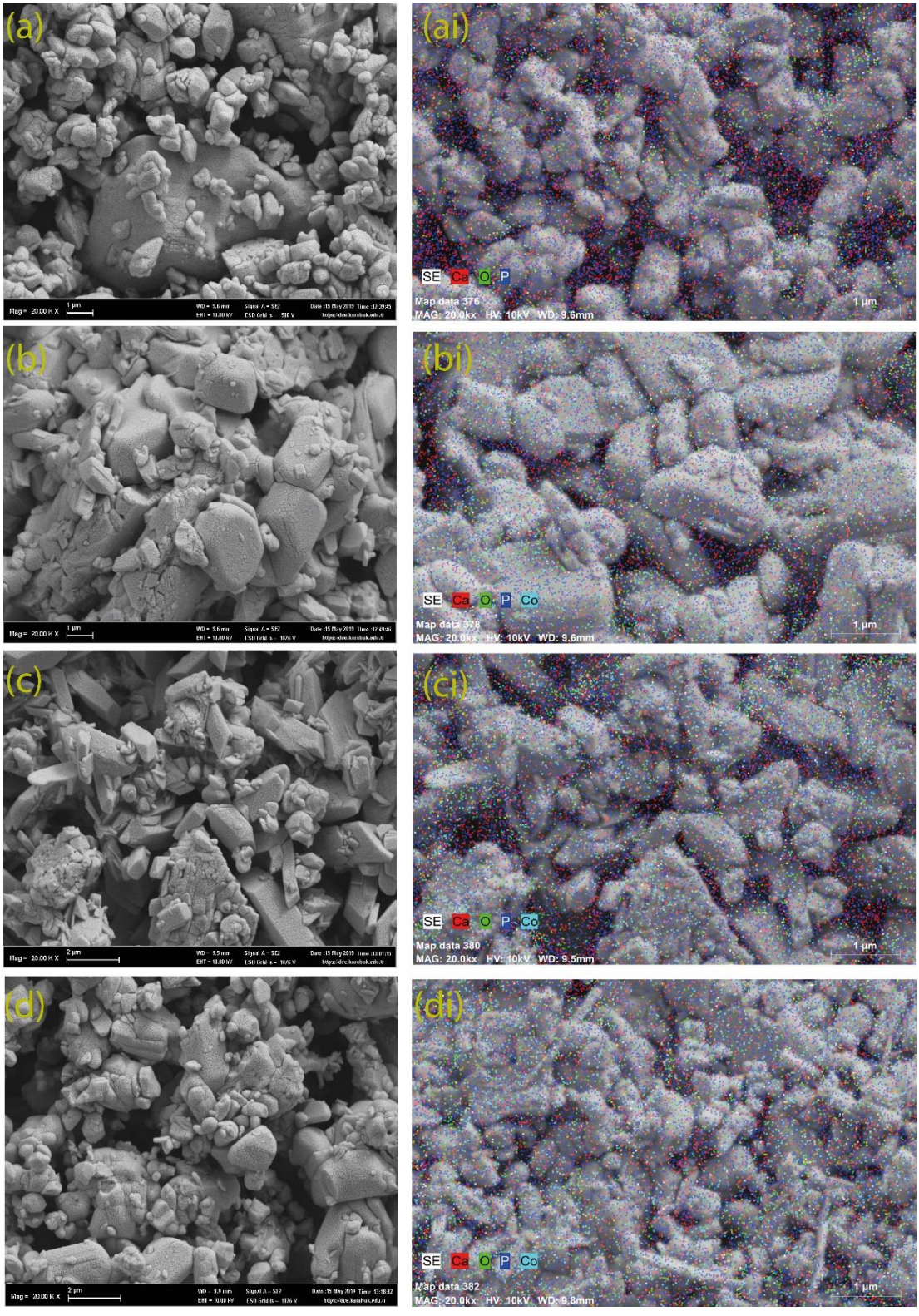

Figure 4.7. SEM images of pure DCP (a), 1Co- DCP (b), 2Co- DCP (c), and 3Co- DCP (d). Elemental mapping of Ca, P, Co, and O elements for pure DCP (ai), 1Co- DCP (bi), 2Co- DCP (ci), and 3Co- DCP (di).

The *in vitro* degradation test was evaluated using PBS over 14 days immersion period. The pH value and leaching profile of Ca, P, and Co ions were measured, and the results are displayed in Figure 4.8 (a-d). After immersion the discs in the PBS, the pH value of PBS decreased upon increasing the immersion period. It further decreased with the incorporation of Co^{2+} ions into DCP cements. (Figure 4.8 (a)). In fact, DCP cement is acidic in nature; also, the leaching of Ca^{2+} and Co^{2+} ions decreased the pH value [111]. The leaching profile of Ca^{2+} ions showed maximum release at day 7 of the incubation period, then declined with prolonged the incubation period to 14 days. The release of Ca^{2+} ions decreased with an addition of Co^{2+} ions (Figure 4.8 (b)). This behaviour could be ascribed to the redeposition of Ca^{2+} ions in the form of new CaP crystals on the surface of monetite cements. The leaching of P ions has no clear trend, and the obtained data were fluctuated (Figure 4.8 (c)). The releasing amount of Co^{2+} increased proportionally to the incorporation amount of Co^{2+} ions into DCP cements (Figure 4.8 (d)), maximum leaching of Co^{2+} was observed at day 14, and it was about 3.69 mg/L. In the previous studies, the rats and mice were exposed to Co in the range of 0.063-6.3 mg. In this test, 6.3 mg was tolerated without toxic behaviour [112].

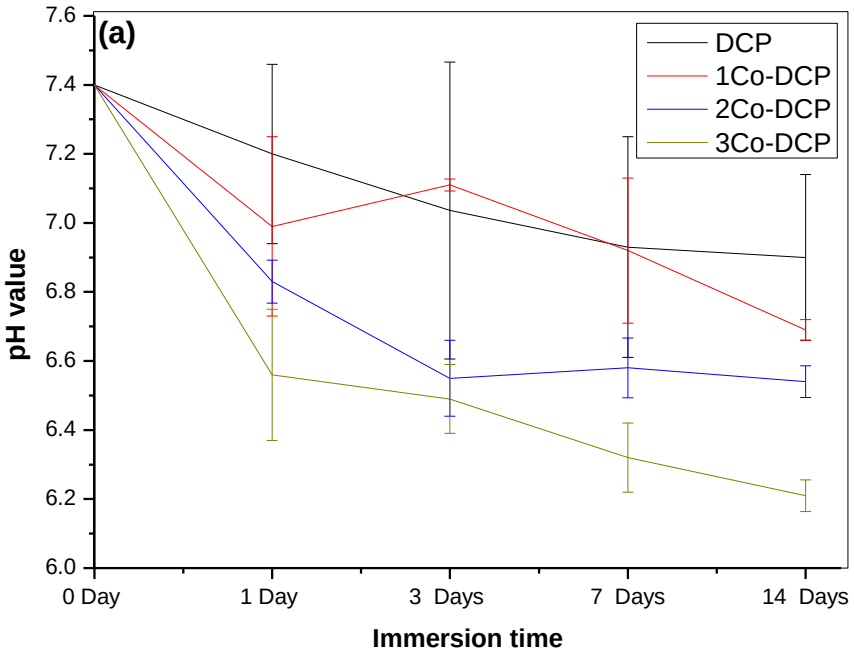

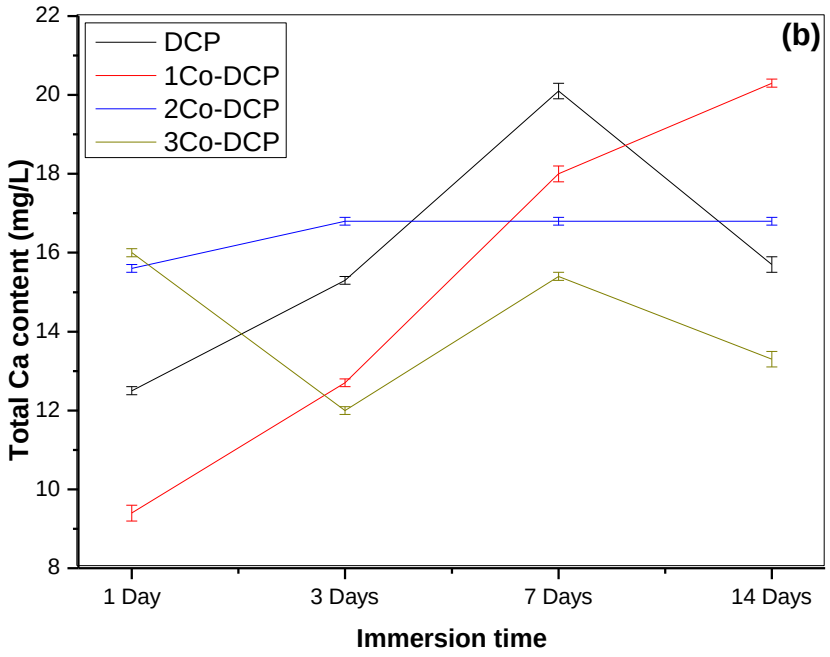
(b)
DCP
1Co-DCP
2Co-DCP
3Co-DCP
Total Ca content (mg/L)
22
20
18
16
14
12
10
8
1 Day
3 Days
7 Days
14 Days
Immersion time

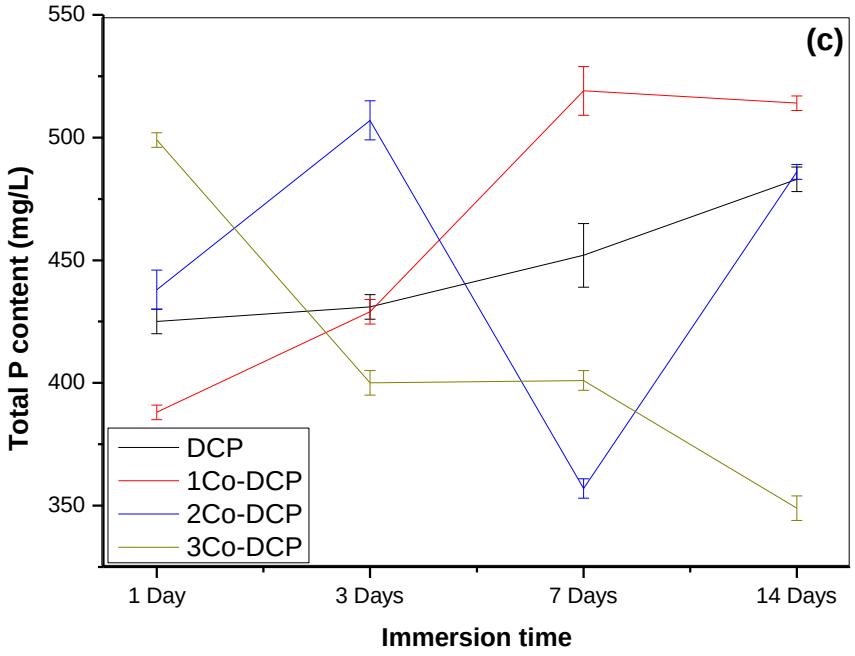
(c)
Total P content (mg/L)
550
500
450
400
350
DCP
1Co-DCP
2Co-DCP
3Co-DCP
1 Day
3 Days
7 Days
14 Days
Immersion time

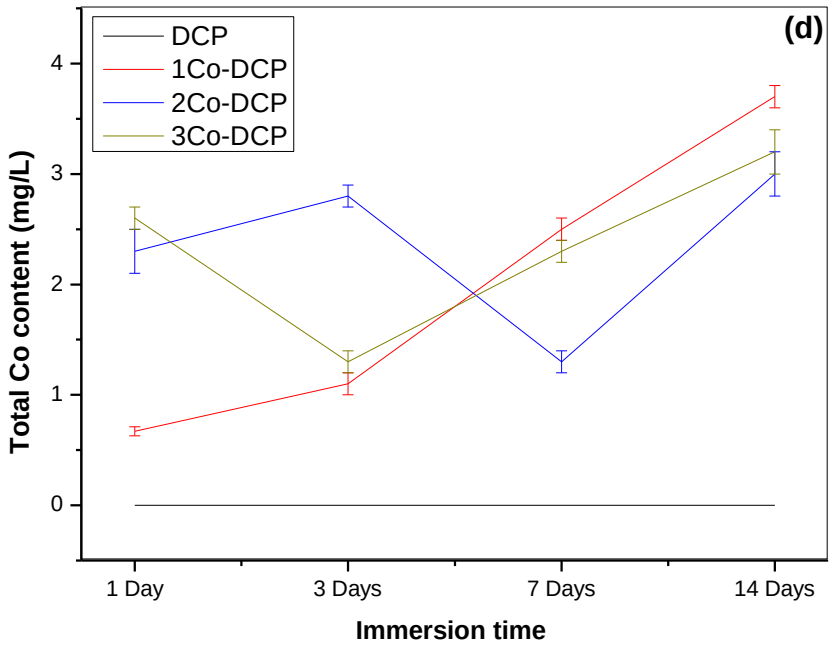

Figure 4. 8. (a) pH value of PBS, (b) total Ca amount, (c) total P amount, and (d) total Co amount for various immersion periods.

Antibacterial properties of pure and Co doped DCP cements were evaluated qualitatively against E.coli, MRSA, MR-CoNS, MSSA, and P. aeruginosa bacteria. The pure phase of DCP and 1Co-DCP (0.78 g of Co^{2+}) ions doped DCP (1Co-DCP) showed no antimicrobial behaviour against the used bacteria. Increasing the doping amount of Co^{2+} ions (2Co-DCP) inhibited the growth of E.coli and MSSA bacteria. The mean diameter of the inhibition zone for E.coli and MSSA bacteria was 19.5 mm, and 23.2 mm, respectively. Furthermore, the inhibition zone increased with an increasing amount of Co^{2+} ions into the DCP structure. The inhibition zone rose to 25.7 mm (E Coli), and 27 mm (MSSA).

This growth inhibitions of E.coli and MSSA bacteria could be ascribed to the leaching of Co^{2+} ions from the surface of Co-DCP cements into the culturing medium, then the positive ions (Co^{2+}) attracted by the negatively charged phosphate and carboxylic group nucleic acids of bacteria cell surface [113]. The accumulation of Co^{2+} on bacteria cell wall leads to an increase in Co^{2+} concentration on the cell

wall, which can subsequently inhibit endogenous respiration of cells as well as penetrate the cytoplasm of the cells via the CorA system (inorganic metal transport) [114,115], resulting in cell death through leakage of intracellular substances. Furthermore, reduction in the pH value of the environment for Co-DCP cements (Figure. 4.8. (a)) could be another factor responsible for the death of bacteria [116].

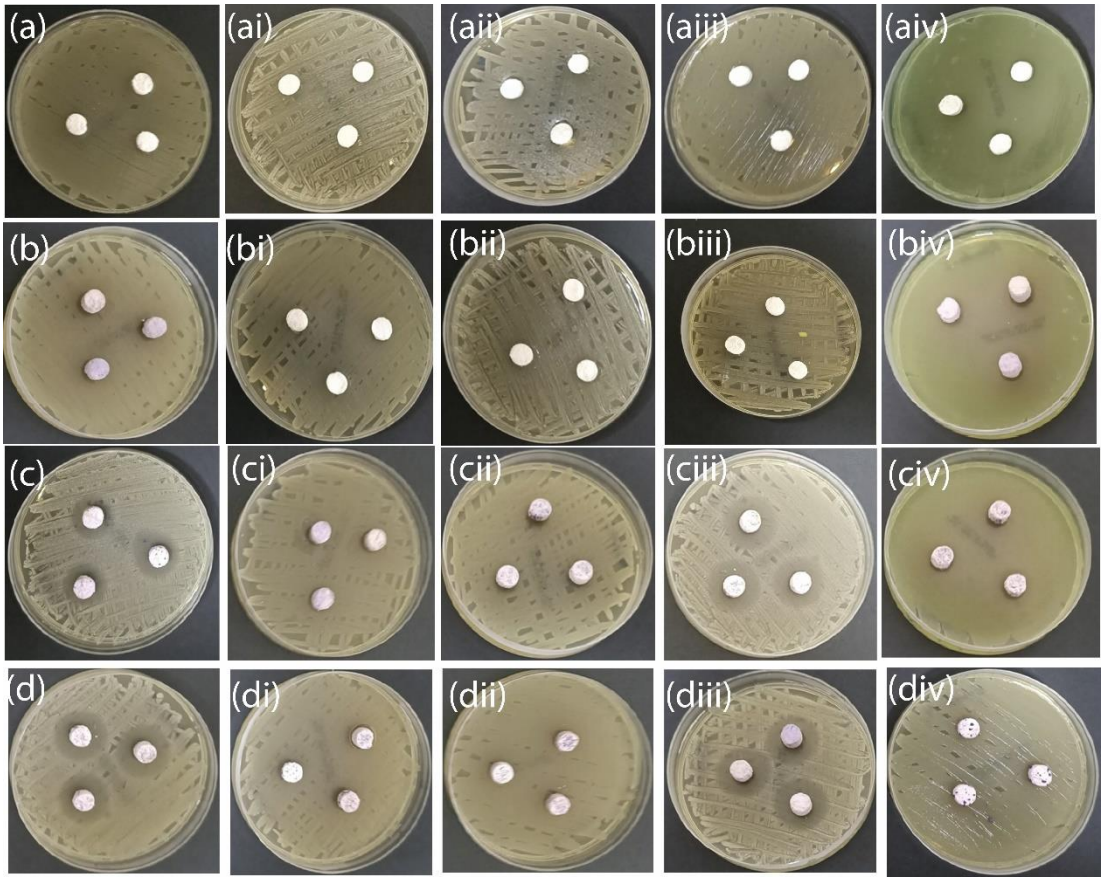

Figure 4.9. (a-aiv) pure DCP cements cultured with E.coli, MRSA, MR-CoNS, MSSA, and P. aeruginosa bacteria, respectively. (b-biv) 1Co-DCP cements cultured with E.coli, MRSA, MR-CoNS, MSSA, and P. aeruginosa bacteria, respectively. (c-civ) 2Co-DCP cements cultured with E.coli, MRSA, MR-CoNS, MSSA, and P. aeruginosa bacteria, respectively. (d-div) 3Co-DCP cements cultured with E.coli, MRSA, MR-CoNS, MSSA, and P. aeruginosa bacteria, respectively. The disc diffusion assay was evaluated for 24 h.

PART 5

SUMMARY

5.1. FINDINGS OF THE STUDY

In this work, a microwave-assisted technique was used to synthesize the pure phase of βTCP and Co^{2+} doped βTCP by using calcium nitrate tetrahydrate, diammonium hydrogen phosphate, and cobalt nitrate as Ca^{2+}, PO_4^{3-}, and Co^{2+} precursors, respectively. The obtained materials were washed, filtered, dried, and calcined at 1000 ºC for 2 h. The βTCP (Co-βTCP) powder is mixed with MCPM powder at a weight ratio of 2:1. The DCP bone cements were prepared by mixing the mixture powder with water at a weight/volume ratio of 1:0.53. The entire materials were characterized, and the *in vitro* degradation behaviour and antimicrobial properties of pure DCP and Co doped DCP bone cements were achieved.

Following are the significant findings of this study:

- The pure phase of βTCP and Co^{2+} doped βTCP materials were successfully synthesized. The lattice parameters, degree of crystallinity, and particle size of βTCP particles were significantly decreased with the addition of Co^{2+} ions. The optical properties of βTCP were improved with the incorporation of Co^{2+} ions.
- The DCP and Co doped DCP bone cements were successfully synthesized. The DCP existed as a monetite phase. The lattice parameters of monetite crystals increased with the addition of Co^{2+} ions. At the same time, the degree of crystallinity and crystallite size significantly decreased with an increasing amount of Co^{2+} ions in the DCP structure.
- *In vitro* degradation of DCP and Co-DCP bone cements was successfully performed. The results demonstrated that the incorporation of Co^{2+} ions decreased the degradation of DCP bone cements.

- The growth of E.coli and MSSA bacteria was inhibited by incorporating Co^{2+} ions into DCP bone cements.

5.2. SUGGESTED FUTURE WORK

The materials prepared in this study have shown good physiochemical and antibacterials properties and are therefore would be a promising material for inhibiting any infection-causing failure in bone repair. However, before using them as biomaterials in medical applications, further studies such as *in vitro* bioactivity, *in vitro* mechanical analysis, and *in vitro* cell culture analysis should be conducted.

REFERENCES

1. Huang, Y.-Z., Xie, H.-Q. and Li, X. (2020) 'Scaffolds in Bone Tissue Engineering: Research Progress and Current Applications', in ***Encyclopedia of Bone Biology***. doi: 10.1016/b978-0-12-801238-3.11205-x.

2. Topaloğlu, U., Aydın KETANİ, M. and Güney Saruhan, B. (2017) Kemik Doku ve Kemikleşme Çeşitleri, ***Dicle Üniv Vet Fak Derg***.

3. Farokhi, M. *et al.* (2018) 'Silk fibroin/hydroxyapatite composites for bone tissue engineering', ***Biotechnology Advances***. doi: 10.1016/j.biotechadv.2017.10.001.

4. Moser, S. A. and Gilbert, S. R. (2014) 'OsteomyeLitis', in ***Pathobiology of Human Disease: A Dynamic Encyclopedia of Disease Mechanisms***. doi: 10.1016/B978-0-12-386456-7.03106-3.

5. Mistry, S. *et al.* (2016) 'A novel, multi-barrier, drug eluting calcium sulfate/biphasic calcium phosphate biodegradable composite bone cement for treatment of experimental MRSA osteomyelitis in rabbit model', ***Journal of Controlled Release***. doi: 10.1016/j.jconrel.2016.08.014.

6. Padrão, T. *et al.* (2021) 'Combining local antibiotic delivery with heparinized nanohydroxyapatite/collagen bone substitute: A novel strategy for osteomyelitis treatment', ***Materials Science and Engineering C***. doi: 10.1016/j.msec.2020.111329.

7. Tao, F. *et al.* (2021) 'Chitosan-based drug delivery systems: From synthesis strategy to osteomyelitis treatment – A review', ***Carbohydrate Polymers***. doi: 10.1016/j.carbpol.2020.117063.

8. Silva, V. *et al.* (2020) 'Therapeutic potential of dalbavancin in a rat model of methicillin-resistant Staphylococcus aureus (MRSA)-osteomyelitis', ***International Journal of Antimicrobial Agents***. doi: 10.1016/j.ijantimicag.2020.106021.

9. Sohn, M. J. and Koo, H. W. (2021) 'Experience on antibiotic-impregnated beads for intracranial epidural infection combined with osteomyelitis', ***Interdisciplinary Neurosurgery: Advanced Techniques and Case Management***. doi: 10.1016/j.inat.2020.101036.

10. Gieling, F. *et al.* (2019) 'Bacterial osteomyelitis in veterinary orthopaedics: Pathophysiology, clinical presentation and advances in treatment across multiple species', ***Veterinary Journal***. doi: 10.1016/j.tvjl.2019.06.003.

11. Siek, D. *et al.* (2017) ‘Evaluation of antibacterial activity and cytocompatibility of α-TCP based bone cements with silver-doped hydroxyapatite and CaCO3’, ***Ceramics International***. doi: 10.1016/j.ceramint.2017.07.131.

12. Madhi, M. *et al.* (2020) ‘Nano-strategies in pursuit of efflux pump activeness in Acinetobacter baumannii and Pseudomonas aeruginosa’, ***Gene Reports***. doi: 10.1016/j.genrep.2020.100915.

13. Kavanagh, N. *et al.* (2018) ‘Staphylococcal osteomyelitis: Disease progression, treatment challenges, and future directions’, ***Clinical Microbiology Reviews*.** doi: 10.1128/CMR.00084-17.

14. Özsoy, Ö.(2010) 'Etken Madde İçeren Kemik Çimentolarının Hazırlanması ve Karakterizasyonu' ***Hacettepe University Institute of Science***

15. Planell, J. A. and Navarro, M. (2009) ‘Challenges of bone repair’, in ***Bone Repair Biomaterials*.** doi: 10.1533/9781845696610.1.3.

16. Gelibolu, N.(2015) 'Farklı Kaynaklardan Üretilmiş Hidroksiapatit Katkısının Kemik Çimentosunun Dayanımına Etkisinin İncelenmesi' ***Yildiz Technical University Institute of Science***

17. Wu, X. X. *et al.* (2021) ‘Long-term antibacterial composite via alginate aerogel sustained release of antibiotics and Cu used for bone tissue bacteria infection’, ***International Journal of Biological Macromolecules*.** doi: 10.1016/j.ijbiomac.2020.11.075.

18. Uskoković, V. *et al.* (2019) ‘Gold is for the mistress, silver for the maid: Enhanced mechanical properties, osteoinduction and antibacterial activity due to iron doping of tricalcium phosphate bone cements’, ***Materials Science and Engineering C*.** doi: 10.1016/j.msec.2018.10.028.

19. Eltohamy, M. *et al.* (2018) ‘Anti-bacterial zinc-doped calcium silicate cements: Bone filler’, ***Ceramics International*.** doi: 10.1016/j.ceramint.2018.04.122.

20. Miola, M. *et al.* (2014) ‘Antibiotic-free composite bone cements with antibacterial and bioactive properties. A preliminary study’, ***Materials Science and Engineering*** *C*. doi: 10.1016/j.msec.2014.06.026.

21. Chaharmahali, R., Fattah-alhosseini, A. and Babaei, K. (2021) ‘Surface characterization and corrosion behavior of calcium phosphate (Ca-P) base composite layer on Mg and its alloys using plasma electrolytic oxidation (PEO): A review’, ***Journal of Magnesium and Alloys*.** doi: 10.1016/j.jma.2020.07.004.

22. Uskoković, V. *et al.* (2019) ‘Calcium phosphate nanoparticles as intrinsic inorganic antimicrobials: In search of the key particle property’, ***Biointerphases*.** doi: 10.1116/1.5090396.

23. Cisneros-Pineda, O. G. *et al.* (2014) 'Towards optimization of the silanization process of hydroxyapatite for its use in bone cement formulations', ***Materials Science and Engineering C.*** doi: 10.1016/j.msec.2014.03.064.

24. Agbeboh, N. I. *et al.* (2020) 'Environmentally sustainable processes for the synthesis of hydroxyapatite', ***Heliyon.*** doi: 10.1016/j.heliyon.2020.e03765.

25. Rey, C. *et al.* (2017) 'Bioactive calcium phosphate compounds: Physical chemistry', in ***Comprehensive Biomaterials II.*** doi: 10.1016/B978-0-12-803581-8.10171-7.

26. LeMaitre, Jacques, Christian Pittet, and David Brendlen. "Pasty or liquid multiple constituent compositions for injectable calcium phosphate cements." ***U.S. Patent*** 7,407,542, issued August 5, 2008).

27. Ma, X. P. and Boccaccini, A. R. (2014) 'Tissue Engineering Using Ceramics and Polymers' ***Tissue Engineering Using Ceramics and Polymers.***

28. LeGeros RZ , Lin S , Rohanizadeh R , Mijares D and LeGeros JP (2003). Biphasic calcium phosphate ceramics: preparation, properties and applications . ***J Mater Sci Mater Med*** 14 , 201 – 9 .

29. Sultana, N. (2013) 'Biodegradable PHBV polymer-based scaffolds for bone tissue engineering', in ***SpringerBriefs in Applied Sciences and Technology.*** doi: 10.1007/978-3-642-34802-0_3.

30. Yang, L. *et al.* (2010) 'The effects of inorganic additives to calcium phosphate on in vitro behavior of osteoblasts and osteoclasts', ***Biomaterials.*** doi: 10.1016/j.biomaterials.2010.01.002.

31. V, G. *et al.* (2016) 'Zinc-releasing calcium phosphate cements for bone substitute materials', ***Ceramics International.*** doi: 10.1016/j.ceramint.2016.08.027.

32. Roy, M. *et al.* (2013) 'Effects of zinc and strontium substitution in tricalcium phosphate on osteoclast differentiation and resorption', ***Biomaterials Science.*** doi: 10.1039/c2bm00012a.

33. Cuneyt Tas, A., Bhaduri, S. B. and Jalota, S. (2007) 'Preparation of Zn-doped β-tricalcium phosphate (β-$CaPO_2$) bioceramics', ***Materials Science and Engineering*** *C*. doi: 10.1016/j.msec.2006.05.051.

34. Yin, X. *et al.* (2002) 'Density functional study of structural, electronic and vibrational properties of Mg- and Zn-doped tricalcium phosphate biomaterials', ***Biomaterials.*** doi: 10.1016/S0142-9612(02)00199-0.

35. De Araujo, T. S. *et al.* (2010) 'Phosphates nanoparticles doped with zinc and manganese for sunscreens', ***Materials Chemistry and Physics.*** doi: 10.1016/j.matchemphys.2010.08.034.

36. Xue, W. *et al.* (2008) 'Synthesis and characterization of tricalcium phosphate with Zn and Mg based dopants', in ***Journal of Materials Science: Materials in Medicine.*** doi: 10.1007/s10856-008-3395-4.

37. Gallo, M. *et al.* (2019) 'Effect of grain orientation and magnesium doping on β-tricalcium phosphate resorption behavior', ***Acta Biomaterialia.*** doi: 10.1016/j.actbio.2019.02.045.

38. Zheng, H. R. *et al.* (2017) 'Effects of MgO modified βTCP nanoparticles on the microstructure and properties of β-TCP/Mg-Zn-Zr composites', ***Bioactive Materials.*** doi: 10.1016/j.bioactmat.2016.12.004.

39. Banerjee, S. S. *et al.* (2010) 'Understanding the influence of MgO and SrO binary doping on the mechanical and biological properties of βTCP ceramics', ***Acta Biomaterialia.*** doi: 10.1016/j.actbio.2010.05.012.

40. Ewald, A. *et al.* (2011) 'Silver-doped calcium phosphate cements with antimicrobial activity', ***Acta Biomaterialia.*** doi: 10.1016/j.actbio.2011.06.049.

41. Zhang, X. *et al.* (1997) 'Toughening of calcium hydroxyapatite with silver particles', ***Journal of Materials Science.*** doi: 10.1023/A:1018568308926.

42. Matsumoto, N. *et al.* (2009) 'Preparation and characterization of β-tricalcium phosphate co-doped with monovalent and divalent antibacterial metal ions', ***Acta Biomaterialia.*** doi: 10.1016/j.actbio.2009.04.010.

43. Yuan, J. *et al.* (2020) 'Nanosized-Ag-doped porous β-tricalcium phosphate for biological applications', ***Materials Science and Engineering C.*** doi: 10.1016/j.msec.2020.111037.

44. Gokcekaya, O. *et al.* (2015) 'Synthesis and characterization of Ag-containing calcium phosphates with various Ca/P ratios', ***Materials Science and Engineering*** *C*. doi: 10.1016/j.msec.2015.04.025.

45. Zhao, L. *et al.* (2011) 'Antibacterial nano-structured titania coating incorporated with silver nanoparticles', ***Biomaterials.*** doi: 10.1016/j.biomaterials.2011.04.040.

46. Wang, Y. *et al.* (2016) 'Antibiotic-loaded, silver core-embedded mesoporous silica nanovehicles as a synergistic antibacterial agent for the treatment of drug-resistant infections', ***Biomaterials.*** doi: 10.1016/j.biomaterials.2016.06.004.

47. Yuan, Z. *et al.* (2018) 'Construction of Ag-incorporated coating on Ti substrates for inhibited bacterial growth and enhanced osteoblast response', ***Colloids and Surfaces B: Biointerfaces.*** doi: 10.1016/j.colsurfb.2018.07.064.

48. Abdalameer, N. K., Khalaph, K. A. and Ali, E. M. (2021) 'Ag/AgO nanoparticles: Green synthesis and investigation of their bacterial inhibition effects', ***Materials Today: Proceedings.*** doi: 10.1016/j.matpr.2021.03.166.

49. Makhetha, T. A. and Moutloali, R. M. (2021) 'Incorporation of a novel Ag–Cu@ZIF-8@GO nanocomposite into polyethersulfone membrane for fouling and bacterial resistance', ***Journal of Membrane Science.*** doi: 10.1016/j.memsci.2020.118733.

50. P Wexler (ed). Encyclopedia of Toxicology, Third Edition. Waltham, MA: ***Academic Press, Imprint of Elsevier***; 2014: pp 5,220. ISBN: 978-0-12-386454-3.

51. Kramer, E., Itzkowitz, E. and Wei, M. (2014) 'Synthesis and characterization of cobalt-substituted hydroxyapatite powders', ***Ceramics International.*** doi: 10.1016/j.ceramint.2014.05.072.

52. Taylor, A. and Marks, V. (1978) 'Cobalt: A review', ***International Journal of Food Sciences and Nutrition.*** doi: 10.3109/09637487809144525.

53. Karunakaran, G. *et al.* (2020) 'Microwave-assisted synthesis of superparamagnetic mesoporous Co-doped hydroxyapatite nanorods for various biomedical applications', ***Ceramics International.*** doi: 10.1016/j.ceramint.2020.11.234.

54. Bhattacharjee, A. *et al.* (2020) 'Antibacterial and magnetic response of site-specific cobalt incorporated hydroxyapatite', ***Ceramics International.*** doi: 10.1016/j.ceramint.2019.08.291.

55. Kargozar, S. *et al.* (2017) 'Strontium- and cobalt-substituted bioactive glasses seeded with human umbilical cord perivascular cells to promote bone regeneration via enhanced osteogenic and angiogenic activities', ***Acta Biomaterialia.*** doi: 10.1016/j.actbio.2017.06.021.

56. Zheng, Y., Yang, Y. and Deng, Y. (2019) 'Dual therapeutic cobalt-incorporated bioceramics accelerate bone tissue regeneration', ***Materials Science and Engineering C.*** doi: 10.1016/j.msec.2019.02.020.

57. Wu, C. *et al.* (2012) 'Hypoxia-mimicking mesoporous bioactive glass scaffolds with controllable cobalt ion release for bone tissue engineering', ***Biomaterials.*** doi: 10.1016/j.biomaterials.2011.11.042.

58. Kulanthaivel, S. *et al.* (2016) 'Cobalt doped proangiogenic hydroxyapatite for bone tissue engineering application', ***Materials Science and Engineering C.*** doi: 10.1016/j.msec.2015.08.052.

59. Wright, J. D. and Sommerdijk, N. A. J. M. (2018) Sol-Gel Materials, Sol-Gel Materials. ***Gordon and Breach Science Publishers*** doi: 10.1201/9781315273808.

60. Ruiz-Aguilar, C. *et al.* (2018) 'Characterization of β-tricalcium phosphate powders synthesized by sol-gel and mechanosynthesis', ***Boletin de la Sociedad Espanola de Ceramica y Vidrio.*** doi: 10.1016/j.bsecv.2018.04.004.

61. Che, J. *et al.* (2021) 'Effects of Mn-doping on the structure and in vitro degradation of β-tricalcium phosphate' ***Journal of Ceramics International.*** doi:10.1016/j.ceramint.2021.05.013

62. Chou, Y. J., Ningsih, H. S. and Shih, S. J. (2020) 'Preparation, characterization and investigation of antibacterial silver-zinc co-doped β-tricalcium phosphate by spray pyrolysis', ***Ceramics International.*** doi: 10.1016/j.ceramint.2020.03.245.

63. Woignier, T. and Phalippou, J. (2016) 'Glasses: Sol–Gel Methods', in ***Reference Module in Materials Science and Materials Engineering*.** doi: 10.1016/b978-0-12-803581-8.02341-9.

64. Boanini, E. *et al.* (2019) 'Strontium and zinc substitution in β-tricalcium phosphate: An X-ray diffraction, solid state NMR and ATR-FTIR study', ***Journal of Functional Biomaterials*.** doi: 10.3390/jfb10020020.

65. A. Bahadır, (2008) 'Gümüş Katkılı Kalsiyum Fosfat Malzemelerden Karmaşık Mimarili Skafolt Fabrikasyonu' ***İstanbul Technical University Institute of Science***

66. Orlovskii, V. P., Komlev, V. S. and Barinov, S. M. (2002) 'Hydroxyapatite and hydroxyapatite-based ceramics', ***Inorganic Materials.*** doi: 10.1023/A:1020585800572.

67. Safronova, T. V. *et al.* (2007) 'Hydroxyapatite-based ceramic materials prepared using solutions of different concentrations', ***Inorganic Materials*.** doi: 10.1134/S0020168507080158.

68. Alshemary, A. Z. *et al.* (2021) 'Biomechanical Evaluation of an Injectable Alginate /Dicalcium Phosphate Cement Composites for Bone Tissue Engineering', ***Journal of the Mechanical Behavior of Biomedical Materials*.** doi: 10.1016/j.jmbbm.2021.104439.

69. Sha, L. *et al.* (2011) 'Microwave-assisted co-precipitation synthesis of high purity β-tricalcium phosphate crystalline powders', ***Materials Chemistry and Physics*.** doi: 10.1016/j.matchemphys.2011.05.075.

70. Iqbal, N. *et al.* (2014) 'Characterization, antibacterial and in vitro compatibility of zinc-silver doped hydroxyapatite nanoparticles prepared through microwave synthesis', ***Ceramics International*.** doi: 10.1016/j.ceramint.2013.08.125.

71. Evis, Z. 'Çeşitli İyonlar Eklenmiş Nano- Hidroksiapatitler: Üretim Yöntemleri, İç Yapı, Mekanik ve Biyouyumluluk Özellikleri Yönlerinden İncelenmesi' (2011) ***Uluslararası Mühendislik Araştırma ve Geliştirme Dergisi*.**

72. Siddharthan, A., Seshadri, S. K. and Kumar, T. S. S. (2006) 'Influence of microwave power on nanosized hydroxyapatite particles', ***Scripta Materialia*.** doi: 10.1016/j.scriptamat.2006.03.044.

73. Goh, K. W. *et al.* (2021) 'Effect of pH on the properties of eggshell-derived hydroxyapatite bioceramic synthesized by wet chemical method assisted by microwave irradiation', ***Ceramics International*.** doi: 10.1016/j.ceramint.2020.12.009.

74. Tariq, U. *et al.* (2019) 'Injectable dicalcium phosphate bone cement prepared from biphasic calcium phosphate extracted from lamb bone', ***Materials Science and Engineering C*.** doi: 10.1016/j.msec.2019.109863.

75. Hasan, M. L. *et al.* (2019) 'In vitro and in vivo evaluation of bioglass microspheres incorporated brushite cement for bone regeneration', ***Materials Science and Engineering C*.** doi: 10.1016/j.msec.2019.109775.

76. Ginebra, M. P. (2008) 'Calcium phosphate bone cements', in ***Orthopaedic Bone Cements*.** doi: 10.1533/9781845695170.2.206.

77. Amer, W. *et al.* (2014) 'Smart designing of new hybrid materials based on brushite-alginate and monetite-alginate microspheres: Bio-inspired for sequential nucleation and growth', ***Materials Science and Engineering C*.** doi: 10.1016/j.msec.2013.11.012.

78. Ji, C. and Ahn, J. G. (2010) 'Clinical experience of the brushite calcium phosphate cement for the repair and augmentation of surgically induced cranial defects following the pterional craniotomy', ***Journal of Korean Neurosurgical Society*.** doi: 10.3340/jkns.2010.47.3.180.

79. Tamimi, F. *et al.* (2009) 'Craniofacial vertical bone augmentation: A comparison between 3D printed monolithic monetite blocks and autologous onlay grafts in the rabbit', ***Biomaterials*.** doi: 10.1016/j.biomaterials.2009.07.049.

80. Hurle, K. *et al.* (2021) 'Ion-doped Brushite Cements for Bone Regeneration', ***Acta Biomaterialia*.** doi: 10.1016/j.actbio.2021.01.004.

81. Cama, G. (2014) 'Calcium phosphate cements for bone regeneration', in ***Biomaterials for Bone Regeneration: Novel Techniques and Applications*.** doi: 10.1533/9780857098104.1.3.

82. Torres, J. *et al.* (2015) 'Monetite granules versus particulate autologous bone in bone regeneration', ***Annals of Anatomy*.** doi: 10.1016/j.aanat.2015.03.008.

83. Tamimi, F. *et al.* (2009) 'Craniofacial vertical bone augmentation: A comparison between 3D printed monolithic monetite blocks and autologous onlay grafts in the rabbit', ***Biomaterials*.** doi: 10.1016/j.biomaterials.2009.07.049.

84. Zhou, H. *et al.* (2021) 'Monetite, An important Calcium Phosphate Compound – Its Synthesis, Properties and Applications in Orthopedics', ***Acta Biomaterialia*.** doi: 10.1016/j.actbio.2021.03.050.

85. Chen, S. *et al.* (2018) 'Eu3+ doped monetite and its use as fluorescent agent for dental restorations', ***Ceramics International.*** doi: 10.1016/j.ceramint.2018.03.068.

86. Motameni, A., Alshemary, A. Z. and Evis, Z. (2021) 'A review of synthesis methods, properties and use of monetite cements as filler for bone defects', ***Ceramics International.*** doi: 10.1016/j.ceramint.2021.01.240.

87. Zhou, H. *et al.* (2021) 'Monetite, an important calcium phosphate compound–Its synthesis, properties and applications in orthopedics', ***Acta Biomaterialia.*** doi: 10.1016/j.actbio.2021.03.050.

88. Saleh, A. T., Ling, L. S. and Hussain, R. (2016) 'Injectable magnesium-doped brushite cement for controlled drug release application', ***Journal of Materials Science.*** doi: 10.1007/s10853-016-0017-2.

89. Cabrejos-Azama, J. *et al.* (2016) 'Magnesium substitution in brushite cements: Efficacy of a new biomaterial loaded with vancomycin for the treatment of Staphylococcus aureus infections', ***Materials Science and Engineering C.*** doi: 10.1016/j.msec.2015.10.092.

90. Alkhraisat, M. H. *et al.* (2013) 'Magnesium substitution in brushite cements', ***Materials Science and Engineering C.*** doi: 10.1016/j.msec.2012.09.017.

91. Rau, J. *et al.* (2016) 'Silver-Doped Calcium Phosphate Bone Cements with Antibacterial Properties', ***Journal of Functional Biomaterials.*** doi: 10.3390/jfb7020010.

92. Vahabzadeh, S. *et al.* (2015) 'IGF-loaded silicon and zinc doped brushite cement: Physico-mechanical characterization and in vivo osteogenesis evaluation', ***Integrative Biology (United Kingdom).*** doi: 10.1039/c5ib00114e.

93. Graziani, V. *et al.* (2016) 'Zinc-releasing calcium phosphate cements for bone substitute materials', ***Ceramics International.*** doi: 10.1016/j.ceramint.2016.08.027.

94. Taha, A. *et al.* (2017) 'Strontium doped injectable bone cement for potential drug delivery applications', ***Materials Science and Engineering C.*** doi: 10.1016/j.msec.2017.05.117.

95. Cummings, H. *et al.* (2017) 'Cobalt-Doped Brushite Cement: Preparation, Characterization, and In Vitro Interaction with Osteosarcoma Cells', ***The Minerals, Metals & Materials Society*** doi: 10.1007/s11837-017-2376-9.

96. Vahabzadeh, S. *et al.* (2019) 'Effects of Cobalt on Physical and Mechanical Properties and In Vitro Degradation Behavior of Brushite Cement', ***The Minerals, Metals & Materials Society*** doi: 10.1007/s11837-018-3204-6.

97. Chen, S. *et al.* (2016) 'Synthesis of Ag doped calcium phosphate particles and their antibacterial effect as additives in dental glass ionomer cements', ***Journal of Materials Science: Materials in Medicine.*** doi: 10.1007/s10856-016-5785-3.

98. Motameni, A. *et al.* (2021) 'Lanthanum doped dicalcium phosphate bone cements for potential use as filler for bone defects', ***Materials Today Communications.*** doi: 10.1016/j.mtcomm.2020.101774.

99. Cama, G. *et al.* (2017) 'The role of new zinc incorporated monetite cements on osteogenic differentiation of human mesenchymal stem cells', ***Materials Science and Engineering C.*** doi: 10.1016/j.msec.2017.04.086.

100. Kozelskaya, A. I. *et al.* (2020) 'Radio frequency magnetron sputtering of Sr- and Mg-substituted β-tricalcium phosphate: Analysis of the physicochemical properties and deposition rate of coatings', ***Applied Surface Science.*** doi: 10.1016/j.apsusc.2019.144763.

101. Tank, K. P. *et al.* (2013) 'Cobalt-doped nanohydroxyapatite: Synthesis, characterization, antimicrobial and hemolytic studies', ***Journal of Nanoparticle Research.*** doi: 10.1007/s11051-013-1644-z.

102. Pang, Y. *et al.* (2020) 'Facilely synthesized cobalt doped hydroxyapatite as hydroxyl promoted peroxymonosulfate activator for degradation of Rhodamine B', ***Journal of Hazardous Materials.*** doi: 10.1016/j.jhazmat.2019.121447.

103. Robles-Águila, M. J., Reyes-Avendaño, J. A. and Mendoza, M. E. (2017) 'Structural analysis of metal-doped (Mn, Fe, Co, Ni, Cu, Zn) calcium hydroxyapatite synthetized by a sol-gel microwave-assisted method', ***Ceramics International.*** doi: 10.1016/j.ceramint.2017.06.154.

104. Girase, K. D. (2013) 'Effect of cobalt doping on FT-IR, raman spectra and thermal stability of lead iodate crystals', ***Journal of Nano- and Electronic Physics.***

105. Grigoraviciute-Puroniene, I. *et al.* (2017) 'A novel wet polymeric precipitation synthesis method for monophasic β-TCP', ***Advanced Powder Technology.*** doi: 10.1016/j.apt.2017.06.014.

106. Motameni, A. *et al.* (2020) 'Lanthanum doped dicalcium phosphate bone cements for potential use as filler for bone defects', ***Materials Today Communications.*** doi: 10.1016/j.mtcomm.2020.101774.

107. Schwarz, M. *et al.* (2016) 'Optoacoustic Imaging of Skin', in ***Imaging in Dermatology.*** doi: 10.1016/B978-0-12-802838-4.00026-1.

108. Shen, Q. *et al.* (2020) 'Recent development of small-molecule organic fluorophores for multifunctional bioimaging in the second near-infrared window', ***Journal of Luminescence.*** doi: 10.1016/j.jlumin.2020.117338.

109. Mondal, S. B. *et al.* (2014) 'Real-time fluorescence image-guided oncologic surgery', in ***Advances in Cancer Research*.** doi: 10.1016/B978-0-12-411638-2.00005-7.

110. Choudhury, B. and Choudhury, A. (2012) 'Luminescence characteristics of cobalt doped TiO2 nanoparticles', ***Journal of Luminescence*.** doi: 10.1016/j.jlumin.2011.08.020.

111. Tang, C. M. *et al.* (2021) 'Effects of electrode plate annealing treatment and the addition of hydrogen peroxide on improving the degradation of cobalt hydroxyapatite for bone repair', ***Materials Chemistry and Physics*.** doi: 10.1016/j.matchemphys.2020.123962.

112. Monnot, A. D. *et al.* (2021) 'A hazard evaluation of the reproductive/developmental toxicity of cobalt in medical devices', ***Regulatory Toxicology and Pharmacology*.** doi: 10.1016/j.yrtph.2021.104932.

113. Burgain, J. *et al.* (2014) 'Lactic acid bacteria in dairy food: Surface characterization and interactions with food matrix components', ***Advances in Colloid and Interface Science*.** doi: 10.1016/j.cis.2014.09.005.

114. Nies, Dietrich H. "Microbial heavy-metal resistance." ***Applied Microbiology And Biotechnology*** 51, no. 6 (1999): 730-750.

115. Alshemary, A. Z. *et al.* (2015) 'Synthesis, characterization, in vitro bioactivity and antimicrobial activity of magnesium and nickel doped silicate hydroxyapatite', ***Ceramics International*.** doi: 10.1016/j.ceramint.2015.06.003.

116. Li, M. *et al.* (2014) 'The antibacterial activity and mechanism of mussel shell waste derived material', ***Powder Technology*.** doi: 10.1016/j.powtec.2014.05.067.

RESUME

Betül SARSIK graduated first and elementary education in Karabuk. She completed high school education in Safranbolu Anatolian Teacher Training High School, after that, she started undergraduate program in Karabuk University Department of Biomedical Engineering in 2012.